MODULATION OF ALPHA-SYNUCLEIN PROTEIN FOLDING BY A MARINE-SOURCED EXTRACT

by

James Christopher Giffin

Submitted in partial fulfilment of the requirements for the degree of Master of Science at

Dalhousie University

Halifax, Nova Scotia

April 2016

TABLE OF CONTENTS

LIST OF FIGURES

ABSTRACT

Protein misfolding has increasingly been recognized to have causative roles in several human neurological diseases. Alpha-synuclein (αS) is a protein involved in the regulation of several neuronal synaptic functions. When misfolded and aggregated into an amyloid form, αS has been implicated in neuronal dysfunction and degeneration in Parkinson's disease and related disorders. The goal of this project was to evaluate the effects of marine species-derived extracts from the Bay of Fundy, Canada, on the melting temperature of αS. Fractions that increased and decreased the α-synuclein melting temperature were identified within a single extract. These fractions were separated by acetone precipitation and size fractionation. The effects of fractions on amyloid formation were assessed. Compounds identified in this way may lead to novel marine-sourced products that directly prevent the protein misfolding that appears to be causative in Parkinson's disease.

LIST OF ABBREVIATIONS AND SYMBOLS USED

Aβ	Amyloid Beta
AD	Alzheimer's Disease
ALS	Amyotrophic Lateral Sclerosis
αS	Alpha Synuclein
BME	β-Mercaptoethanol
BS^3	Bis(sulfosuccinimidyl) Suberate
BOG	N-Octyl-β-D-Glucoside
CD	Circular Dichroism
EGCG	Epigallocatechin 3-Galate
HD	Huntington's Disease
HEPES	4-(2-Hydroxyethyl)-1-Piperazineethanesulfonic Acid
MES	2-(N-Morpholino)Ethanesulfonic Acid
NACP	Non Amyloid Component Precursor Protein, or Alpha Synuclein
NDGA	Nordihydroguaiaretic Acid
PD	Parkinson's Disease
SOD1	Superoxide Dismutase 1
SDS	Sodium Dodecyl Sulfate
TEM	Transmission Electron Microscopy
TFMSA	Trifluoromethanesulfonic Acid
ThT	Thioflavin T
T_m	Melting Temperature
TRIS	Tris(Hydroxymethyl)Aminomethane

ACKNOWLEDGEMENTS

I thank Dr. Vanya Ewart for all her support. From the NRC, I thank Bob Richards for his guidance and training; Cheryl Craft, Shawna King and Nusrat Jahan for their help with preparing the extracts; and Cindy Leggadrio and Dave O'Neil for their training on transmission electron microscopy. I thank my committee members Dr.Tom MacRae, Dr. Neil Ross and Dr. Brian Stavely for their insight and comments for preparing the final submission. I thank my wife Morgan for helping with corrections.

CHAPTER 1 INTRODUCTION

1.1 Amyloid

1.1.1 Protein Folding and Misfolding

Proteins are covalent polymers of amino acids and the order of amino acids in the polymer is the amino acid sequence. The amino acid sequence of a protein is its primary structure; however, many protein regions associate within themselves to form secondary structures that are stabilized by non-covalent interactions. The two most common secondary structures are α-helix and β-sheet. The α-helical structure is defined as a right-handed coil with hydrogen bonding between carbonyl groups and amine groups along the backbone of the coil. The β-sheet structure is defined as a set of planar strands of protein joined by at least three hydrogen bonds between the backbones of adjacent strands. A small structure is the compact β-turn, which allows an abrupt change of direction in a peptide chain and, in the absence of defined structure, the peptide chain is referred to as random coil or as unstructured. Proteins can further fold into tertiary structures that are formed by combinations of secondary structures; the tertiary structure is normally called the conformation or the fold of the protein. Although most proteins have tertiary structure, a minority of proteins are natively disordered; they are completely unstructured in their functional state. An example of a protein with a well-studied tertiary structure is ribonuclease A. Ribonuclease A has secondary structure elements that include β-sheet, turns, bends and α-helices (Kartha, Bello, Harker 1967; Kover et al. 2008). A diagram of the ribonuclease primary sequence and secondary structure is shown in Figure 1 (Kover et al. 2011).

Natively disordered proteins, as well as those with defined secondary and tertiary native structures, may adopt a non-native folded structure, which is called misfolding. Proteins misfold due to enzymatic cleavage, post-translational modification, mutation, overabundance or structural destabilization due to alteration in the tissue environment. Normally, cells can recognize and dispose of misfolded proteins, either through targeted degradation in the proteasome or refolding with the help of chaperone proteins (Chen et al. 2011; Douglas and Dillin 2010), but some misfolded proteins form aggregates i*n vivo* that are not amenable to disassembly and refolding or to proteolysis and these cause problems. Cells lose the functionality of the soluble protein after protein aggregation and the aggregates may be toxic, either of which can lead to disease.

Amyloid is the name of a peptide expressed in brain that forms aggregates that stain with iodine. This staining initially led the aggregates to be called “amyloid”, which means “starch-like (Virchow 1854). However, subsequent studies revealed that the aggregates are formed by a peptide, which was then named amyloid beta (Aβ). The Aβ peptide aggregates revealed a highly stable and tightly-folded association of β-sheets (Eanes and Glenner 1968) called cross-beta structure, which polymerizes into fibrils. Cross-beta tertiary structures similar to that of the aggregated Aβ peptide are formed by many other proteins. Therefore, this cross-beta structure is referred to as an amyloid fold or amyloid structure in any protein that converts to it

A

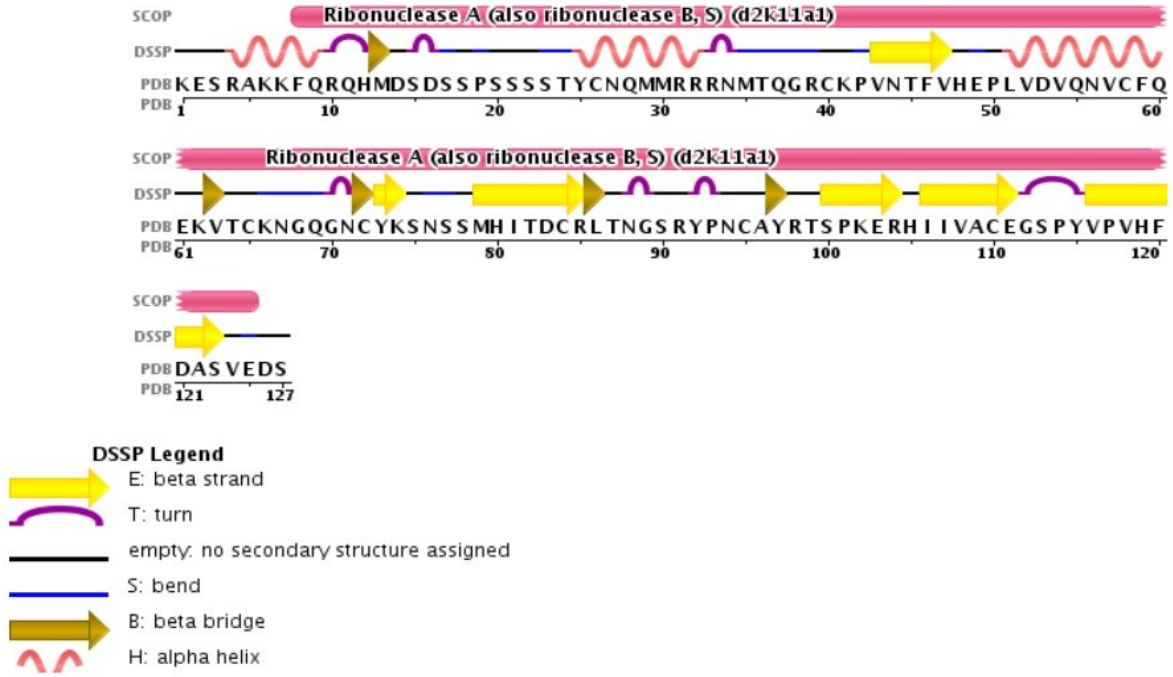

B

Figure 1: Secondary and tertiary structure of ribonuclease. Both diagrams were taken from PDB entries generated previously (Kover et al. 2011). Panel A: “Define secondary structure of protein” (DSSP) is an algorithm for predicting the secondary structure of a string of amino acids based on their physical properties. Panel B: In the tertiary structure diagram, the orange color represents beta strands, pink represents alpha helices and white portions are loops or bends.

through misfolding (Chiti and Dobson 2006). The term amyloid will therefore be used in this thesis to refer to this folding structure in any protein, rather than to the Aβ peptide specifically.

Viewed with transmission electron microscope, amyloid appears fibrous, with substantial variation in fibril abundance and length. This is far more informative than the "starch-like" appearance of the amyloid aggregates (plaques) when viewed under light microscopy (Kyle 2001). The presence of amyloid is detected and even quantified *in vitro* with Congo red (Puchtler, Sweat, LeVine 1962), thioflavin T (ThT), and thioflavin S (Kelienyi 1967; LeVine 1999). Amyloid consists of small peptides or proteins that form a tightly wound beta structure, and it extends easily by addition of protein units to form visible fibers and clumps (Kyle 2001). Extensive study into the morphology of amyloid fibrils has been done and the fibers are composed of small protofilaments, which are in turn comprised of β-sheet stacked in an antiparallel fashion. This tertiary fold is the cross-beta structure noted above, and perpendicular to the long axis of the meta fiber (Serpell et al. 2000; Sunde and Blake 1997). A number of different amyloid forming proteins were studied by Serpell et al. (2000), including immunoglobulin l light chains, Leu60Arg variant apolipoprotein AI, amyloid A protein (AA), and Asp67His variant lysozyme. Serpell et al showed that there were between 2 and 6 protofilaments in a large amyloid fiber and each amyloid protofilament was 2-5 nm in diameter (Serpell et al. 2000). Under certain circumstances, amyloid is used in cells for specialized purposes (Chiti and Dobson 2006). The actinobacterium *Streptomyces coelicolor* uses the protein ChpD-H to form amyloid fibers (Claessen et al. 2003). These fibers allow the bacteria to form a hydrophobic surface where water meets air and allow the hyphae of the bacteria to grow in air by coating the outside of the hyphae in hydrophobic fibers (Claessen et al. 2003). Furthermore,

cultured human melanocytes regulate the cleavage of an intraluminal protein Pmel17, resulting in a peptide that is incorporated into an amyloid-like fibril upon which melanins are deposited (Berson et al. 2003). While it seems that the amyloid fold may have adaptive roles in some contexts, the majority of known amyloid formation, particularly those occurring in mammals, are detrimental.

1.1.2 Amyloid Formation and Human Disease

Protein misfolding is currently recognized as a central pathogenic event in a large number of human neurodegenerative diseases where the proteins responsible adopt non-functional folds. In some proteins, the misfolded structure forms aggregates and if the aggregates are amyloid, toxicity results. Normally, when a protein misfolds it is targeted for degradation by the proteostasis network, or refolded by chaperone proteins (De Strooper 2010; Morimoto 2008). If a misfolded protein is degraded, the cell is not damaged. However, proteins that misfold into amyloid pose a particular problem. The amyloid conformation provides a structural template upon which further misfolding of the same protein can occur, drawing monomers out of solution into a growing and propagating aggregate (Lotz and Legleiter 2013). Therefore, further growth occurs. In other words, over time, and if not destroyed, the amyloid aggregate serves as a locally infectious template, causing other natively folded proteins to misfold on its surfaces until it large fibrils are formed, which clump into plaques. This is reminiscent of prions.

The idea of proteins as disease-transmitting agents is relatively recent. Until about 30 years ago, it appeared that bacteria and viruses were responsible for the majority of human disease, and it

was only after extensive study of animal encephalopathies that it was postulated that infection could spread without nucleic acid (Alper et al. 1967). When studying the infectious agent causing scrapie and related diseases, Pruisner and colleagues discovered that toxic proteins were propagating through templating (Diener, McKinley, Prusiner 1982). The term prion, a combination of the words protein and infection, was coined (Diener, McKinley, Prusiner 1982). A prion is a misfolded protein that infects a healthy cell or organism by converting endogenous prion proteins to the toxic form. Prions misfold into an amyloid structure that induces the same misfolding in neighboring prion proteins (Costanzo and Zurzolo 2013).

A number of neurodegenerative diseases have "prion-like" characteristics, in that the misfolded aggregates move from cell to cell, allowing spread of the pathogenic protein to other parts of tissues in which they are located (Costanzo and Zurzolo 2013; Frost and Diamond 2010). In Alzheimer's disease (AD), Huntington's disease (HD), amyotrophic lateral sclerosis (ALS) and Parkinson's disease (PD), key misfolded proteins are respectively Aβ, huntingtin, superoxide dismutase (SOD) and α synuclein (αS) (Chiti and Dobson 2006). AD accounts for the majority of dementia cases, making it the most common neurodegenerative disease (Nussbaum and Ellis 2003). AD is characterized on a molecular level by extracellular aggregates of Aβ oligomers and plaques and intracellular neurofibrillary tangles. There is increasing evidence that the Aβ oligomers are responsible for the observed toxicity in AD, which leads to cognitive deficits in reasoning, memory, abstraction, and eventually motor skills. As AD progresses, the patient suffers cognitive decline until death. Huntington's disease is caused by an excessive number of sequential glutamines near the N terminus of the protein huntingtin. An expansion of the natural glutamine stretch exceeding approximately 33 residues results in progressive loss of muscle

coordination and cognitive function. The age of onset of the disease declines with increasing residue number (Andrew et al. 1993; Snell et al. 1993). As described for Aβ above, misfolded huntingtin forms amyloid (Jayaraman et al. 2012). A likely reason for this is the increased propensity for aggregation with increasing polyglutamine length through a collapsed conformation (Walters and Murphy 2009). In contrast to Huntington's disease, ALS is associated with the death of the upper and lower motor neurons in the spinal cord, brain stem and motor cortex. The dying neurons contain aggregate protein inclusions that may be responsible for cell death. Mutant forms of SOD1 (Kerman et al. 2010) and TAR DNA binding protein (TDP-43) (Guo et al. 2011) are found in these aggregates along with ubiquitin (Deng et al. 2011). SOD misfolding may be common to all forms of ALS (Pokrishevsky et al. 2012). Interestingly, SOD appears to misfold, aggregate and act as a template for further SOD misfolding without adopting a detectable amyloid fold (Kerman et al. 2010). Therefore, the amyloid fold is not strictly required for prion-like propagation. PD is the subject of the next section and it is discussed in depth there.

1.2 Parkinson's Disease

PD affects the substantia nigra, a region of the brain involved with reward, addiction and movement. Many of the onset symptoms of PD reflect its effects on the substantia nigra and diagnosis is based on resting tremor, bradykinesia, rigidity, and postural instability (Hoehn and Yahr 1967) resulting from a lack of the neurotransmitter dopamine in the striatum of the brain due to the loss of cells in the substantia nigra, where dopamine is produced. The majority of PD cases are sporadic and some of those may be environmentally induced. In two separate studies

that controlled for cigarette smoking and in which smoking was a benfit, exposure to agricultural chemicals such as paraquat (Liou et al. 1997), organochlorines and alkylated phosphates (Seidler et al. 1996) increased the risk of PD. There was an increased likelihood of PD in patients who had experienced severe head trauma, but this was not dose-dependent (Seidler et al. 1996). Rat models of PD employ the pesticide rotenone to induce PD.

PD is related to the misfolding of αS into aggregates found in Lewy bodies and Lewy neurites (Nussbaum and Ellis 2003), described more completely in the next section. The prion-like spread of misfolded αS and concomitant increase in PD symptoms over time in healthy mice injected with small doses of misfolded fibrils point to a direct role for αS (Luk et al. 2012). Furthermore, healthy non-human primates can be infected with PD upon injection of Lewy body fractions extracted from PD patients (Rescasens, Ariadna et al. 2013). For these reasons, a key focus of PD research is the αS protein.

1.2.1 Alpha Synuclein

1.2.1.1 Structure

The protein αS was originally found in amyloid rich Alzheimer's plaques as the non-amyloid beta (Aβ) component (NAC), a 35 amino acid fragment (Ueda et al. 1993). The NAC fragment was linked to its precursor protein, NACP, of 140 amino acids and shortly afterwards two proteins similar to the rat torpedo synuclein were isolated from human brain tissue, one of them, identical to NACP and referred to as αS (Jakes, Spillantini, Goedert 1994). A recent study

spanning 73 organisms containing αS, beta-synuclein and gamma-synuclein concluded that gamma-synuclein is likely to be the common ancestor for both of the others, and that the novel secondary copper-binding region in αS noted below is highly conserved among variants of the protein (Yuan and Zhao 2013). A secondary copper binding region is located between E46K and A53T of αS, two well know mutations leading to early onset PD (Yuan and Zhao 2013).

The NAC fragment of αS is a strongly hydrophobic stretch of amino acids from 60 to 95 and it is essential for αS misfolding (Giasson et al. 2001). αS has an amphipathic lysine-rich amino terminus and a disordered, acidic carboxy-terminal tail. The amino terminus is acetylated (Kang et al. 2012). Interestingly, the acetylated species of αS has a higher propensity to fold into a helical structure, rather than aggregate (Kang et al. 2012; Trexler and Rhoades 2012). The physiological role of the acetylation of αS is not understood. The carboxy-terminal tail of αS is involved in nuclear localization as well as interactions with small molecules, metals and proteins. There is a primary binding site for copper II on the amino terminus located at His-50 that accelerates the aggregation of αS at physiological concentrations (Rasia et al. 2005). The amphipathic region is likely involved in membrane association, and responsible for the partial alpha helical structure observed upon interaction with artificial membranes and detergents (Eliezer et al. 2001; Ulmer et al. 2005). Tertiary structure models from two separate studies showing the membrane bound helical structure are displayed in Figure 2, along with a secondary structure prediction diagram. αS has several helical conformations when interacting with membranes, which include a long helical stretch and a broken helix joined by an exposed linker region (Drescher, Huber, Subramaniam 2012; Wietek et al. 2013). Lokappa et al. (2011) showed that αS switched between the two different membrane-bound helical conformations, and

membrane bound αS likely exists in a 7.6:1 equilibrium between long helix and broken helix conformations (Lokappa and Ulmer 2011). The natural degradation of αS occurs by proteosomal mechanisms and by autophagy (Webb et al. 2003).

αS was originally thought to be a naturally unfolded monomer, as a result of studies on αS expressed in *Escherichia coli* (Weinreb et al. 1996) but more recent studies show that αS exists as a membrane-bound α helix, or as a α helical tetramer in its native form (Bartels, Choi, Selkoe 2011; Eliezer et al. 2001). A subsequent investigation of αS structure suggested that αS as α helical tetramer migrates at a size of about 60 kDa, which is consistent with the expected size of a monomer in an extended conformation (Fauvet et al. 2012). This does not rule out the possibility of a native, functional multimer, but the protein must be further characterized. Fold stabilization of native αS, whether it is slightly disordered, α helical, or some other stable native fold, is recognized as a key strategy to prevent the transition to a toxic amyloid form (Lashuel et al. 2013).

A

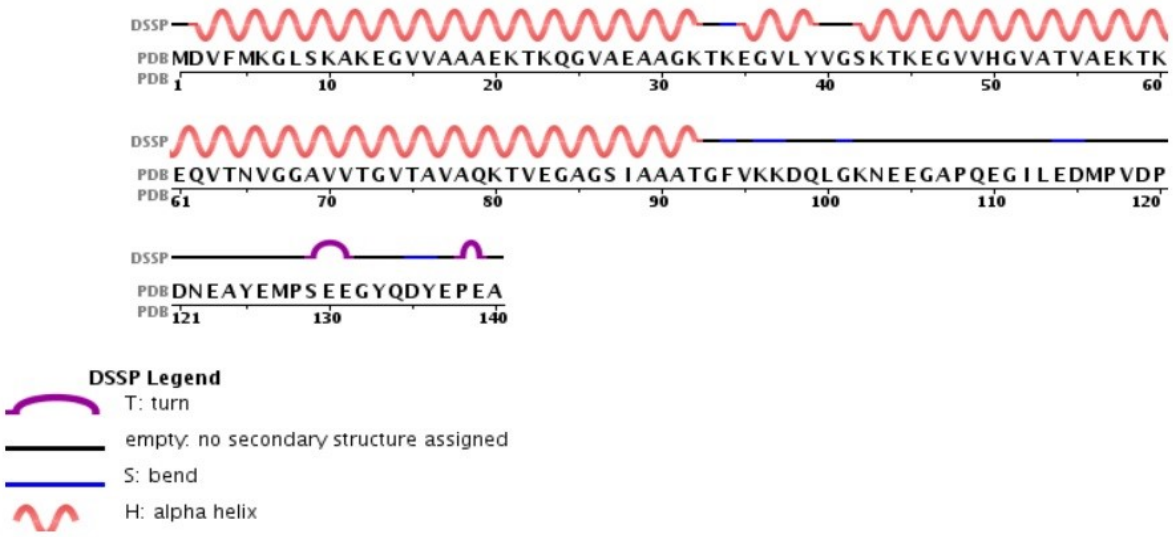

B

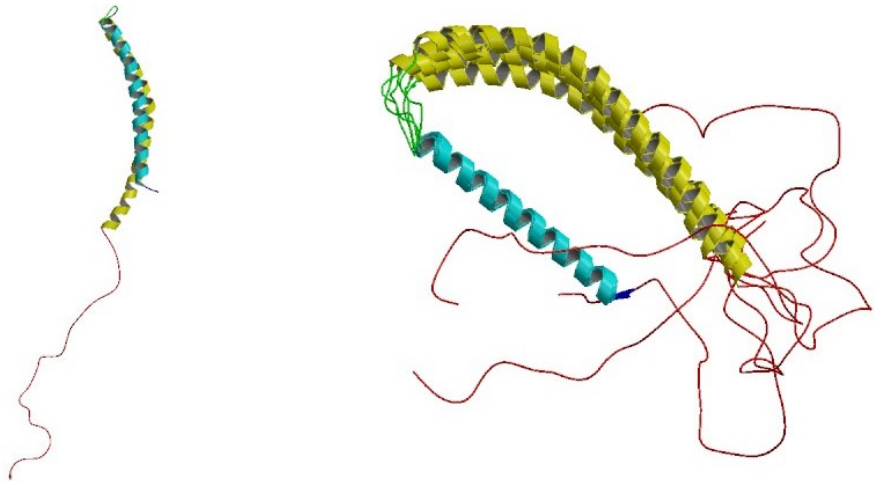

Figure 2: The sequence and structure of αS. Panel A shows the sequence of αS along with the secondary structure depicted as line patterns. Panel B shows two images of partially folded structures for αS. The structure on the left is the α helical micelle bound αS 1XQ8 (PDB) (T. Ulmer, Bax, Cole, & Nussbaum, 2005) and the one on the right is αS to which the detergent sodium laurel sarcosinate (SLAS) is bound (Rao, Jao, Hegde, Langen, & Ulmer, 2010). The NAC fragment is 60-95 of αS which is the last yellow helix structure before the random coil.

1.2.1.2 Function

The biological role of αS is not completely understood. αS is produced in neurons and red blood cells (Barbour et al. 2008; Weinreb et al. 1996). Although the role of αS in red blood cells is unknown, there are several clues as to its role in neurons. αS is localized in a specific subpopulation of synaptic vesicles in neurons (Kahle et al. 2000) and when αS is absent or overproduced, problems with sustained synaptic transmission arise with repetitive stimulation (Abeliovich et al. 2000; Cabin et al. 2002). αS appears to be involved in refilling the pools of neurotransmitters at the site of synaptic transmission from the distal reserve pool of neurotransmitters. Abeliovich et al. (2000) showed that brains from mice lacking αS had reduced striatal dopamine, but no change in dopamine release or reuptake. Subsequently, Cabin et al (2002) examined brain tissue from αS knockout mice using transmission electron microscopy and found that there were fewer undocked vesicles in neurons, while docked vesicles remained unaltered. The normal dopamine response to repetitive stimuli was also impaired in these knockout mice (Cabin et al. 2002). This supports the idea that αS regulates refilling of dopamine from reserve pools to the site of synaptic release. The mouse knockouts used in both studies were viable, with unaltered dopaminergic cell bodies, fibers and synapses. That dopamine response is altered on repetitive stimuli in αS knockouts, along with the lack of effect on a single electrical stimulus, supports the idea that αS is not directly affecting dopamine signaling. Instead in PD, it appears that the amyloid aggregates of αS, whether as small oligomers or in the larger Lewy bodies, are toxic to the neurons that harbor them (Spillantini et al. 1997). Dopamine appears to interact with αS (Planchard et al. 2014) however, the significance of this interaction in cells is

not yet clear. A physiological role for αS in brain may be fostering the assembly of soluble N-ethylmaleimide–sensitive factor attachment protein receptor (SNARE) complexes, which have a role in neurotransmitter release (Burre et al. 2010). Synuclein-knockout mice showed impaired SNARE complex assembly and reduced lifespan (Burre et al. 2010), suggesting an important role for synucleins in healthy neurons.

1.2.2 Mechanism of Amyloid Folding in Disease-Causing Proteins

Although PD and other neurological diseases involving misfolded proteins appear to have prion-like features of templates spreading misfolded conformations to their native counterparts, the question remains as to how the initial amyloid conversion begins. Although neurological diseases vary in prevalence, some, such as Huntington's appear to be exclusively genetic, whereas others such as PD and ALS appear to be primarily sporadic. Mutations in specific proteins increase the likelihood of neurodegenerative diseases. In many cases, mutation favours formation of the misfolded state, this is the case with the extra polyglutamine repeats in the huntingtin protein chain (Walters and Murphy 2009). In familial ALS, 11 missense mutations in SOD-1 are linked to the disease (Rosen et al. 1993). AD is linked heritably to a single point mutation in APP, valine to isoleucine at position 717 (Goate et al. 1991). Another mutation in the AD3 gene, is thought to contribute to altered transport or processing of APP which could lead to its interaction with tau (Sherrington et al. 1995). Missense mutations, repeats and gene duplications all cause proteins to become toxic. In each case, either the protein that misfolds is overproduced, altered in a manner that favours misfolding, transported incorrectly, or allowed to persist as a result of damage to the cell's proteostasis network.

In some cases, PD is inherited and there are several known mutations that are associated with increased incidence of PD. An example of this is a threonine substitution for alanine at position 53 (A53T) (Polymeropoulos et al. 1997). This mutation is autosomal dominant and it causes early onset PD. The Ala residue is within the region that forms α helical structure upon interaction with membranes; the mutation causes a β sheet to be favoured (Polymeropoulos et al. 1997). Increased risk of PD occurs for replacement of the alanine at position 30 with proline (A30P) (Kruger et al. 1998). The possibility that mutations are involved in seemingly sporadic PD has been suggested. Larger studies are needed to confirm the idea, but A18P and A29S have been identified in a Polish subject group of late onset PD (Hoffman-Zacharska et al. 2013). Two of the previously identified inherited mutations of αS, A53P and E46K, are in a Cu^{2+}-binding region of the helical secondary structure and it was postulated that impairment of copper binding contributes to misfolding (Yuan and Zhao 2013).

The proteins involved in neurodegenerative disease all have functional roles in the brain when folded normally, or in some cases natively unfolded. Under normal conditions, proteins that misfold are handled by the proteostasis network. Action by the proteostasis network can include refolding by chaperone proteins, degradation by the ubiquitin proteasome system and/or directed to the lysosome for recycling (Glickman and Ciechanover 2002; Levine and Klionsky 2004). Impaired refolding and clearing of aberrant proteins allow these proteins to persist and nucleate oligomers. This appears to have a role in the early AD symptoms of Down's syndrome, which usually occur after the age of 40. When brain tissue samples from patients with Down's syndrome were analyzed post mortem by redox proteomics, it was found that the proteostasis

network is impaired in patients younger than 40 who had yet to manifest AD symptoms (Di Domenico et al. 2013). Redox proteomics has recently been used to show that proteome perturbations are an important factor in several other chronic diseases (Butterfield and Dalle-Donne 2012).

Once pathological misfolding has occurred, the proteostasis network is likely further impaired by the accumulation of misfolded protein (Morimoto 2008). Aggregating proteins may inhibit the proteasome (Bence, Sampat, Kopito 2001). For example, the introduction of two unrelated misfolding proteins such as huntingtin fragments containing polyglutamine repeats and a folding mutant of cystic fibrosis transmembrane conductance regulator result in substantial inhibition of the ubiquitin-proteosome system (Bence, Sampat, Kopito 2001). Gradual overburdening of the proteostasis system may contribute to the lag phase of neurodegenerative disease onset and its subsequent rapid progression. It is worth exploring how quickly and completely each of the misfolded proteins suppresses the proteasome because some neurodegenerative diseases progress quite quickly, such as ALS, whereas others such as AD and PD take more time.

1.3 Potential Parkinson's Disease Treatments

1.3.1 Current Research

Neurodegeneration involves a collection of incurable diseases. There are several classes of potential treatments for neurodegenerative diseases, including those that lessen the effects of the

disease, those that modify the course of the disease and finally those that reverse the disease. At this time, the only approved treatments are those that mitigate the symptoms of PD. There are, however, several promising research avenues to pursue in disease modification and reversal of the damage caused by the disease.

Currently, the first line of treatments for PD patients is dopamine replacement therapy. This includes levodopa and carbidopa. Levodopa is the immediate biosynthetic precursor to dopamine (Yahr et al. 1969) and it is converted into dopamine throughout the body by L-amino acid decarboxylase. A number of side effects occurs when treating patients with levodopa, some of which are caused by breakdown of dopamine outside the blood brain barrier (Fahn et al. 2004). An inhibitor of L-amino acid decarboxylase is often prescribed as a combination therapy in order to limit breakdown of dopamine in the periphery. The drug, carbidopa, does not cross the blood brain barrier, so it does not interfere with production of dopamine, which is needed by those with PD. This first line of treatment alleviates symptoms, while disease progression is unaffected.

A different approach to symptom alleviation is deep brain stimulation (DBS), a surgical procedure in which two electrodes are surgically implanted in a patient's brain (Bronstein et al. 2011). Electrical impulses are sent to the thalamus and globus pallidus to block signals responsible for tremor and rigidity. It is not known how this stimulating impulse blocks signals responsible for these symptoms. DBS is meant to be a last resort in patients who have had significant loss in quality of life. Some patients are able to see modest reduction in symptoms with DBS. Like dopamine replacement, this is a treatment that is not disease modifying as the progression of PD is not affected.

A third type of treatment, now in clinical trials is neural grafting, in which dopamine-producing neurons differentiated from embryonic stem cells are implanted into a patient's brain to replace dysfunctional parts of the substantia nigra. This surgery presents risks, including new motor side effects called graft-induced dyskenisia (GIS) or cancer from undifferentiated stem cells (Brundin, Barker, Parmar 2010). More recently, dopamine-producing neurons were cultured from stem cells (Kirkeby et al. 2012), a much more sustainable source of tissue, and even directly from keratinocytes, skipping the stem cell phase altogether (Parmar and Jakobsson 2011). Ideally, culturing neurons from keratinocytes would circumvent some of the risk associated with neural grafts, as well as ethical issues from using embryonic stem cells. The skin cells could be donor matched or even patient specific, allowing higher success rates. If this treatment were successful it would be an example of disease modification. Patients who have had this neural graft relapse 10 years after treatment (Brundin, Barker, Parmar 2010). This could be due to original deposits of misfolded αS spreading from diseased cells through the new tissue, as any original deposits left in the brain would likely be infectious (Luk et al. 2012).

Treatments showing great promise *in vitro*, in cell culture and in small animal models are antiaggregation molecules, the idea being that a molecule with chaperone-like activity is administered to breakup misfolded protein or to stabilize the membrane bound state of the protein. As of yet, no drugs of this class have passed clinical trials. A recent *in vitro* study showed dose dependent inhibition of fibril formation and dose dependent destabilization of preformed fibrils (Ono, Hirohata, Yamada 2007). A molecule with antiaggregation activity is curcumin, a compound present in turmeric. While effective *in vitro*, it is quickly broken down at

physiological pH. Curcumin by-products were evaluated for antiaggregation activity, and of the many tested, biphenyl analogues of dehydrozingerone, and O-methyl-dehydrozingerone have antiaggregation activity (Marchiani et al. 2013). Mannitol is an effective antiaggregation agent *in vivo* in studies in the *Drosophila* PD model (Shaltiel-Karyo et al. 2013).

In *C. elegans* synthesizing Aβ, curcumin and ThT prevent paralysis that is normally caused by the buildup of Aβ (Alavez, Vantipalli, Zucker, Klang, & Lithgow, 2011). In this study, the proteostasis network, specifically heat shock proteins, were required for the beneficial effects caused by the antiaggregation molecules (curcumin, ThT). Additionally, DAF-16, a transcription factor implicated in proteostasis and aging of worms, is required for the benefits of anti-aggregation to ensue. A sample of compounds have significant antiaggregation activity *in vitro* and *in vivo* (mice, worms and cultured cells), but have not had success in human trials yet. The compounds are listed in the next section 1.3.2. There are a growing number of studies employing animal models for neurodegenerative diseases exposed to inhibitors of aggregation that show promising results, as will be discussed in the section on αS.

The best option for treatment of neurological disease could lie in combination therapy. Combining drugs of different actions may be sufficient to restore normal protein homeostasis and reverse the pathological state. Examples of treatments that could be used together in the future are neural grafts for disease modification, dopamine replacement therapy for symptoms, antiaggregation molecules to remove residual misfolded proteins, vapromil to activate inducible chaperone network proteins and rapamycin (Webb et al. 2003) to induce autophagy. A combination of therapies is likely needed to fully reverse a neurological disease because small

amyloid seeds will promote the formation of more misfolded protein. Another aspect of PD treatment that needs study is how well certain treatments will work on PD sufferers with inherited early onset PD versus sporadic mutation based PD or even PD caused by some unknown environmental effects such as lifetime exposure to pesticides. It is likely that a patient with inherited early onset PD must continue treatment indefinitely because the conditions for amyloid seeding are always present.

1.3.2 The Use of Natural Products in Treatments

Hypothesized routes for protein misfolding are outlined for Aβ and αS (Figures 3, 4). There are several promising antiaggregation molecules for Aβ that have been tested *in vitro* and in animal studies and these are outlined on the diagram, along with their proposed actions. A number of these antiaggregation molecules have been tested on αS as well, and sites for possible action on the folding pathway of are outlined in Figure 3, denoted by a *. One of the more commonly mentioned antiaggregation molecules is curcumin (Yang et al. 2005). Curcumin caused a dose-dependent inhibition of Aβ oligomer fibril formation, as shown in both *in vitro* protein studies and *in vivo* mouse models (Yang et al. 2005). Additionally, cucumin bound and unfolded intact Aβ fibrils. This interaction with Aβ was not sequence dependent but appeared to involve recognition of the fibril structure (Yang et al. 2005). Recognition of the structure rather than the sequence means that molecules that inhibit or reverse one type of amyloid structure may also be effective against others. Nordihydroguaiaretic acid (NDGA) protects hippocampal neurons against Aβ toxicity (Goodman et al. 1994).

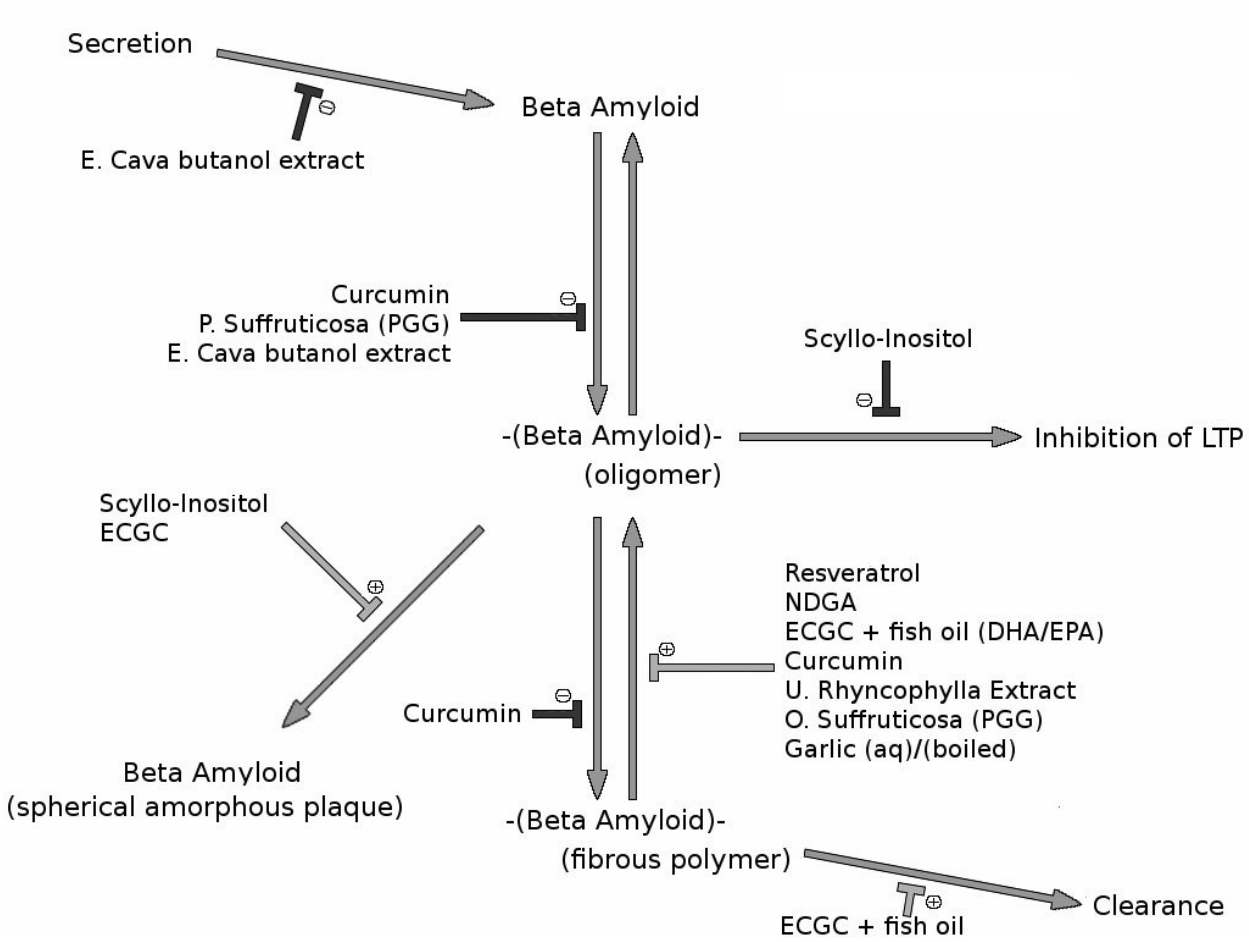

Figure 3: Folding pathways for Aβ illustrating the steps at which selected natural products may act. Several studied antiaggregation agents are highlighted. They are as follows; *Ecklonia cava* extract, curcumin, PGG, scyllo-inositol, ECGC, resveratrol, NDGA, DHA/EPA, *U. rhyncophylla*, and garlic extract.

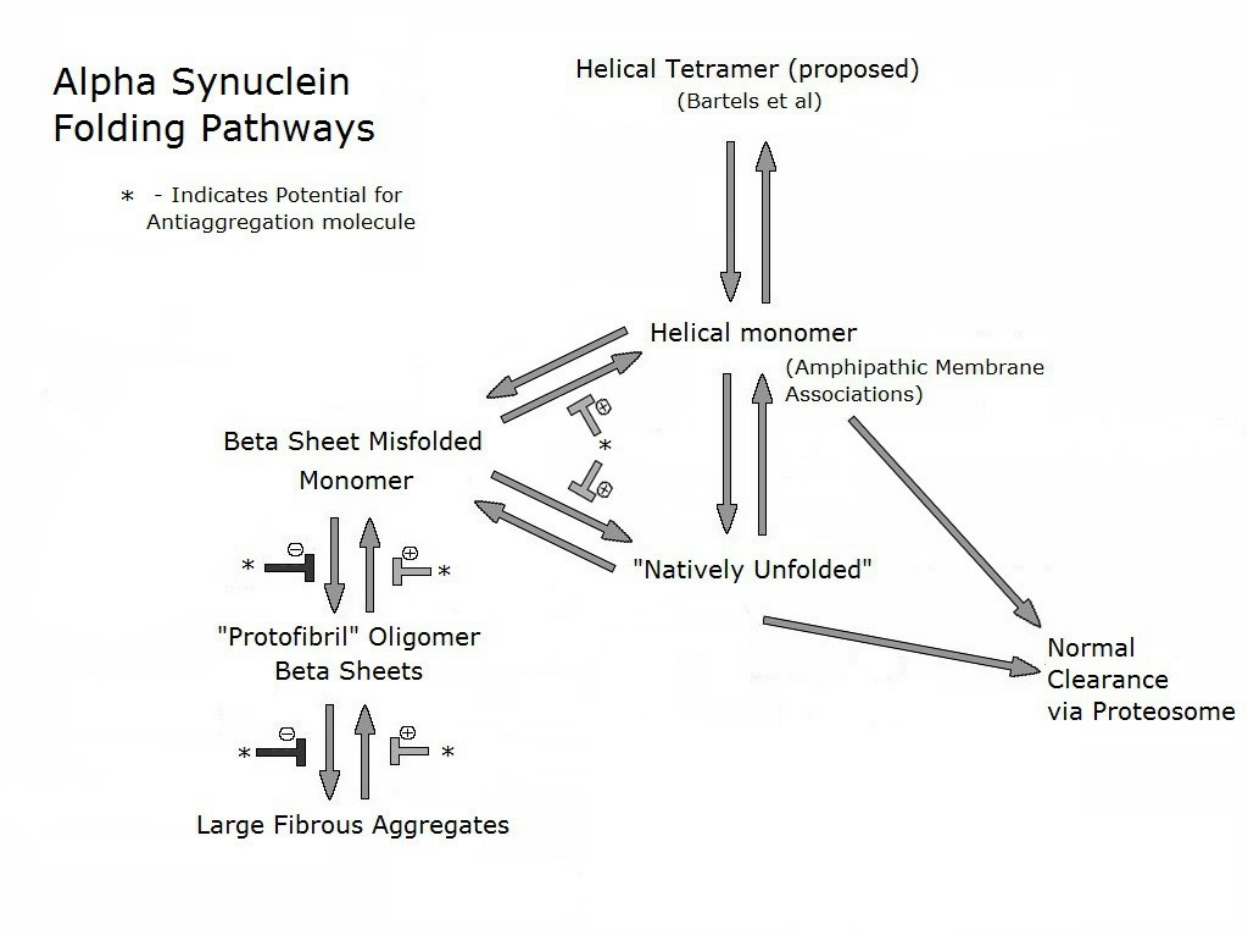

Figure 4: Folding pathways for αS. Stars denote possible sites for the action of antiaggregation agents.

In a later study, NDGA was shown to inhibit formation of Aβ oligomers and aggregates as well as break down preexisting fibrils (Ono et al. 2002). A few other recently studied antiaggregation molecules include *Ecklonia cava* extract (Kang et al. 2011), PGG (Fujiwara et al. 2009), scyllo-inositol (McLaurin et al. 2000), resveratrol (Marambaud, Zhao, Davies 2005), DHA/EPA (Giunta et al. 2010), U. rhyncophylla (Fujiwara et al. 2009), and garlic extract (Gupta, Indi, Rao 2009). These compounds, and the processes they affect, are illustrated in Figure 3. Although all of the compounds noted here were studied in relation to Aβ specifically (Yang et al. 2005), their binding could be unrelated to sequence and dependent on the amyloid fold. Figure 4 shows a similar map for αS, and highlights the hypothetical sites of action for antiaggregation molecules

1.3.3 Cold Adaptation

The ocean is an interesting and promising source of new bioactives for action against neurodegenerative disease due to natural selection for cold adaptation (Dube 2012). Much of the world's oceans are cold, with 90% of ocean water below 5 degrees Celsius (Dube 2012; Storey and Storey 2004). Cold poses a significant stress to organisms living in the ocean, and therefore a significant evolutionary pressure (Pucciarelli et al. 2009; Schulte 2014). Low temperature challenges the ability of proteins to remain folded and the need for molecular chaperones makes the screening of organisms from marine sources particularly relevant for compounds able to combat disease caused by misfolded protein (Pucciarelli et al. 2009).

Many marine species in the North Atlantic are known to be edible, which may increase the likelihood of compounds extracted from them to be safe due to the species established safety as food. A few of the many changes to organisms as a result of temperature stress include "profound alterations to many essential molecular and cellular phenomena, such as energy metabolism, protein stability and transport, mitosis and cytokinesis, assembly of macromolecular complexes, membrane fluidity, and secretory processes (Feller and Gerday 2003; Hochachka and Somero 2002; Pucciarelli et al. 2009)". When this information is applied to the context of protein misfolding in mammalian organisms at a higher temperature, it is apparent that we need to look to these cold adapted organisms for chaperones or antiaggregation molecules.

1.4 Algae

1.4.1 Macroalgae of the North Atlantic Ocean

Algae are a diverse group of photosynthetic aquatic eukaryotes. Microalgae are primarily unicellular organisms, whereas macroalgae are complex multicellular formations. There are four main types of macroalgae in the North Atlantic Ocean; Chlorophyta (green algae), Rhodophyta (red algae), Bacillariophyceae (diatoms) and Phaeophyceae (brown algae). Chorophyta are a large group of algae that are green in colour because they contain a and b chloroplasts in proportions similar to terrestrial plants (Guiry 2014a). Higher plants emerged from this large diverse group of green algae (Palmer, Soltis, Chase 2004). Rhodophyta are a large group of marine multicellular algae (Freshwater et al. 1994) which includes dulse and nori, both used as food (Guiry 2014a). Bacillariophyceae are a major group of algae usually with bilateral

symmetry and central sternum (Guiry 2014a). Phaeophyceae, or brown algae, are the algae of interest in this project. Both algae species the extracts used in this project were made from, *Alaria esculenta* and *Saccharina latissima*, are brown algae. *A. esculenta*, known as winged kelp or dabberlocks, is an edible brown seaweed (Bischof, Hanelt, Wiencke 1999; Guiry 2014a). *A. esculenta* has yellow-brown fronds stretch up to 4 m long and they reach 25 cm in width. *A. esculenta* is attached to rock, usually with a root-like holdfast at the base, and its usual habitat is exposed rock in shallow water or tide pools (Greville 1830; Guiry 2014a). *S. latissima*, known as sea belt, poor man's weather glass and sugar wrack (Guiry 2014a), grows to 3 m in length and has a claw like holdfast and is harvested in Ireland by some for use as konbu (edible kelp) (Guiry 2014b; Reid et al. 2013).

In experiments that led to this thesis research, extracts were prepared from algae obtained by Dr. Thierry Chopin and his team (University of New Brunswick) along with Ms. Cheryl Craft, Dr. Nusrat Jahan and Dr. Shawna MacKinnon (NRC). In preliminary analyses carried out by Dalhousie University Department of Biology Honours Student, Peter Goddard, 16 extracts from the two species of algae were tested for their effect on the folding stability of αS monitored by changes in melting temperature (T_m) of αS using methods very similar to those described in Chapter 2, but with a more rapid temperature increase (Figure 5) There were no significant increases in T_m with any of the algal extracts; however, extract 5 was selected for further study because the highest mean T_m was obtained for the protein under study in its presence.

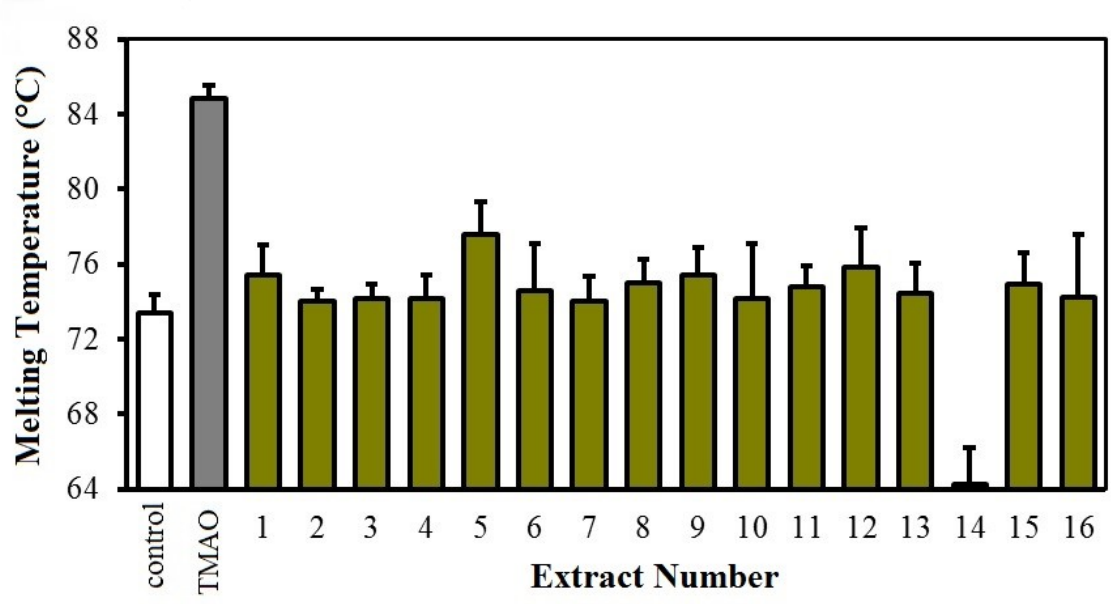

Figure 5: The melting temperature (T_m) of αS in the presence of algal extracts, as determined by SYPRO Orange fluorescence. The unfolding of 0.1 mg/mL αS was measured in 0.1 M MES and in the presence of 1mM SDS. Negative control (white) is the T_m of αS without additions. Positive control (grey) is the T_m of αS in the presence of TMAO, a chemical chaperone. Descriptions of the buffers and solution components listed here are given in Chapter 2.

1.5 Research Objectives

1.5.1 Modulation of Alpha Synuclein Folding by an Algal Extract

The goal of this thesis project was to determine the effects of a marine algal extract on amyloid formation by αS. Extracts prepared by a natural products chemistry team from samples collected by marine biologists were examined using a suite of *in vitro* assays to determine their effects on αS. An active extract was identified and then further studied.

The specific objectives of the project were to address the following questions:

(1) Do these marine algal extracts affect the thermal stability of αS?

(2) Do changes in thermal stability of αS affect amyloid formation?

(3) Does the extract or components thereof, affect αS secondary structure? Are the proportions of secondary structure present related to the amyloid formation?

Taken together, the answers to these questions may provide an understanding of the effects of an algal extract and its fractions on the formation of amyloid by αS. Furthermore, the results will allow a fuller understanding of αS folding behaviour and more complete information on the predictive value of thermal stability changes in identifying amyloid modulating agents. Ultimately, the results will indicate whether the algae studied harbor compounds with the potential for preventing or modifying the progress of PD.

CHAPTER 2: METHODS

2.1 Preparation of Materials

2.1.1 Preparation of Algal Extracts

Samples were prepared from two species of macroalgae obtained from the Bay of Fundy, New Brunswick, Canada by Dr. Thierry Chopin, University of New Brunswick. The species sampled were *A. esculenta* and *S. latissima*, and they were both sourced from Charlie Cove, NB and Maces Bay, NB, on June 15, 2011.

Extracts were prepared by Dr. Shawna MacKinnon, NRC. Seaweed samples were cleaned of dirt and other organisms, rinsed with distilled water, freeze-dried and then ground to a fine powder using a mill. Twenty grams of each seaweed powder was extracted with MeOH/water (1:1) at 50 °C with stirring for 2 h at room temperature. This mixture was then centrifuged to obtain a clarified supernatant. The methanol was removed from the supernatant using rotary evaporation, and the remaining supernatant transferred to vials, freeze-dried and weighed.

Extracts were taken from each algal sample in 75% methanol. Algal extracts were prepared to 50 $mg \cdot mL^{-1}$ and were stored frozen at -20 °C until analysis. When aliquots were prepared for analysis, thawed solution was centrifuged approximately 45 s on a low-speed tabletop minicentrifuge to remove insoluble material and the supernatant was recovered.

Following preliminary studies described in the Introduction, extract 5 was selected for further examination. This extract was obtained from *A. esculenta* collected in Charlie's Cove, NB.

2.1.2 Preparation of αS and Assay Buffer

Recombinant human αS was purchased as a lyophilized powder from rPeptide. A master solution of 2 mg/mL of protein was prepared by adding 500 µL of tissue culture water (Sigma) to the αS. Thirty µL samples were prepared from this master protein solution and stored at -20 °C in PCR tubes. The buffers used in most experiments were 2-(N-morpholino)ethanesulfonic acid (MES) and 4-(2-hydroxyethyl)-1-piperazineethanesulfonic acid (HEPES) and 1M stocks of these were prepared, divided into 1 mL aliquots and frozen at -20 °C until use.

2.2 Thermal Shift Assay

2.2.1 Thermal Shift Measurement

The thermal shift assays employed Sypro Orange (Sigma-Aldrich) as a fluorescent dye that responds differently to folded and unfolded protein. Protein solutions containing Sypro Orange were prepared in white 84 well microplates and then placed in a Roche LightCycler 480 real time PCR machine, which quantified fluorescence as temperature changed. The excitation wavelength was 470 nm and the emission wavelength at which fluorescence was measured was measured at 570 nm; the temperature range used was 25-85 °C, with a ramp speed of 1.26 degrees per

minute. This ramp speed was slower than the qPCR software was designed to allow; it was achieved by setting the number of reads per degree sufficiently high to limit the ramp speed to that sought for these experiments. The Tm was determined using the Roche LightCycler software, which plotted the negative derivative of fluorescence after each experiment. The rate of change in fluorescence was greatest at the T_m, so the location of a dip in the curve was indicative of T_m. The peak change in fluorescence was manually annotated for each well, and the results were then analyzed using Excel software. The peak change in fluorescence was manually annotated for each well by selecting the peak in the area of greatest change after which the results were analyzed using Excel software.

The assay using SYPRO Orange dye (Bio-Rad) was evaluated using carbonic anhydrase II (Sigma) and the LightCycler 480 real time PCR machine (Roche) to ascertain that quantifiable results were achievable in this system. To evaluate the assay, a known carbonic anhydrase chaperone trifluoromethanesulfonic acid (TFMSA) was used over a concentration range of 0 to 120 μM. Solutions were mixed up in a white 96 well PCR plate to a final volume of 20 μL. The concentrations of each part were made to be as follows; tris(hydroxymethyl)aminomethane (TRIS) buffer 0.1M; 2 mM Sodium dodecyl sulfate (SDS); 2 mg/mL carbonic anhydrase ; and SYPRO diluted to 1:300. A different concentration of TFMSA was added to each column on the PCR plates, with duplicate rows for each concentration. SYPRO fluorescence was measured at 470 nm excitation/ 570 nm emission starting at 25°C and at every degree up to 80°C. The assay parameters, including temperature range, assay timing and buffer composition were optimized for αS (rPeptide). Two buffers (MES and HEPES) were tested over a range of concentrations and SDS was evaluated in a similar manner.

2.2.2 Preparation of Assay Solutions

Preliminary thermal shift assays for the analysis of αS were carried out to optimize buffer and detergent concentrations. The buffer, 100 mM 2-(N-morpholino)ethanesulfonic acid (MES) buffer, pH 6.0 was evaluated for suitability in fold analysis of αS, as it had been used previously in several studies of αS (Lee et al. 2012). Sodium dodecyl sulfate (SDS) was tested at 0.25, 0.75, 1.00, 1.50 and 2.00 mM. A second buffer, 100 mM (4-(2-hydroxyethyl)-1-piperazineethanesulfonic acid (HEPES) buffer, pH 7.4, containing 10% glycerol and 150 mM NaCl was evaluated (Bartels, Choi, Selkoe 2011). For the solution containing HEPES, the detergent n-octyl-beta-D-glucoside (BOGS) at concentations of 1, 2, 3, 4 and 10 mM was used. As a positive control, trimethylamine oxide (TMAO) was added to 1 mg/mL αS in 100 mM MES, 1 mM SDS and SYPRO Orange dye. The TMAO was added at the following concentrations; 62.5, 125, 250, and 375 mM. Stock solutions of 1 M MES at pH 6.0, 10 mM SDS and 1:300 SYPRO Orange were prepared in advance and stored at 4°C. The αS, received as a lyophilized powder, was dissolved to 2mg·mL^{-1} (0.139 mM) in water, separated into 30 µL samples and frozen at -20 °C. Tissue culture-grade water was used for all dilutions. The algal extract was obtained at a concentration of 50 mg·mL^{-1} and diluted to 2 mg·mL^{-1} (4 µL extract in 96 µL water) for the assay. Four dilutions yielding 2, 1, 0.4, 0.1, and 0.04 mg·mL^{-1} were made in succession. All tubes of extract were centrifuged briefly prior to use, as described above.

For all experiments, duplicate wells were used. The final concentrations of each component of the extract based thermal shift assays were 100 mM MES, 1 mM SDS, 0.0138 mM αS, and an

extract from 20 $\mu g \cdot mL^{-1}$ to 1000 $\mu g \cdot mL^{-1}$. The plate was centrifuged for 10 seconds in a microplate centrifuge and then placed in the Roche qPCR machine for analysis.

2.2.3 Fractionation of Algal Extract 5

2.2.3.1 Acetone Precipitation

Prior to acetone precipitation of the algal extract, 1.7 mL polypropylene microcentrifuge tubes were treated with acetone in order to remove acetone-soluble impurities. For this purpose, microcentrifuge tubes were soaked in glass-distilled acetone for 24 h. The acetone was discarded and the soak was repeated. Then, the treated tubes were dried and 500 µL fresh acetone was added to each. The acetone precipitation was carried out according to a protocol provided by Pierce Biotechnology. The pretreated tubes of acetone were cooled to -20 °C. Algal extract 5 was diluted to 2 mg/mL in a separate polypropylene microcentrifuge tube (4 µL of the 50 mg/mL extract and 96 µL Pierce tissue culture water) and transferred to tubes of cold acetone such that the proportion of acetone to extract was 4:1 and the final volume was 500 µL. The tube was then vortexed and incubated for 1 h at -20 °C. After incubation, the tube was centrifuged for 10 min at 13,000 g in a microcentrifuge. The supernatant was transferred to another treated microcentrifuge tube. The supernatant was placed in a vacuum centrifuge and dried at 45 °C. Once dry, the material was dissolved in 100 µL of tissue culture water. The pellet obtained from acetone precipitation was dried at room temperature for 30 min after removal of the supernatant and then dissolved in 100 µL of tissue culture water. Both supernatant and pellet solutions were aliquoted and stored frozen at -20 °C until use.

2.2.3.2 Pepsin Digestion

Immobilized pepsin beads (Thermo Scientific) were used to digest any traces of protein that might remain in the algal extracts. The digestion was carried out according to the manufacturer's protocol. The digestion buffer was 20 mM sodium acetate, pH 4.5, prepared in tissue culture water. To equilibrate the pepsin beads in the digestion buffer, 25 µL of gently mixed slurry was added to a 1.7 mL microcentrifuge tube containing 400 µL digestion buffer, mixed, centrifuged at 1000 g for 5 minutes and then the buffer was discarded. This wash step was repeated with another 400 µL digestion buffer, and then the beads were resuspended in 50 µL buffer.

The extract sample was diluted to 100 µL of 1 mg/mL in tissue culture water (Sigma). This sample was added to the tube containing the pepsin beads and incubated at 37 °C for 4 hours in a shaking water bath. After the incubation, the tube was centrifuged for 5 minutes at 1000 g. These digested samples were then ready to be used in the thermal shift assay. To ensure that the pepsin was active, the same digestion was run using bovine serum albumin, carbonic anhydrase II and the mixture of proteins present in the PageRuler™ Prestained Protein Ladder (Thermo Scientific). Digestion products were analyzed by sodium dodecylsulfate polyacrylamide gel electrophoresis (SDS-PAGE) to determine if the pepsin was fully active and completely digesting the protein substrates under the conditions used. Refer to section 2.3 for details on SDS-PAGE methods.

2.2.3.3 Size Fractionation

Size fractionation of the algal extract was carried out by Cheryl Craft and Dr. Nusrat Jahan of NRC. Fractions were prepared by ultrafiltration of the algal extract at a concentration of 46 mg/mL in 25% MeOH/water and using an Amicon Ultra-15 spin (10,000 mass cutoff) filter, followed by an Amicon Ultra-4 (5000 mass cutoff). The fraction retained on the 10,000 mass cutoff filter was re-filtered on an identical filter in order to reduce possible carryover from the mixed portion between 5000 and 10,000. The clean size fractions below 5000 and above 10,000 were designated 5A and 5B, respectively.

2.3 Thioflavin T Binding Assay

Thioflavin T is a benzothiazole dye that binds specifically to the β sheet-rich amyloid structure (LeVine 1993; LeVine 1999). ThT assays were performed as previously described (Dube 2012). Briefly, the experiment was performed as follows. Under low light, a 50 mM stock solution of ThT dye was prepared in distilled water and filtered through a 0.45 μm syringe filter into a 10 mL polycarbonate tube (Falcon). This stock was maintained in the dark, covered in foil at 4°C for up to one month. For the ThT assay a working solution of dye (50 μM ThT, 50 mM glycine-NaOH at pH 8.5), was prepared by adding 1 μL of the stock solution to 1 mL of 50 mM glycine-NaOH, pH 8.5.

For the study of αS, 30 µL incubation mixtures were prepared in water containing a final concentration of 0.1 mg/mL αS in 100 µM MES, pH 6.0, with 1 mM SDS. For the treated tube, extract 5 was added to a final concentration of 1 $mg \cdot mL^{-1}$. The extract was spun for 50 seconds as described in the thermal shift assay prior to first use. These tubes were then incubated at 37 °C, shaking at approximately 200 rpm, for specific time intervals, along with controls. Then, 10 µL of the incubated αS solutions were added to the wells of a black, flat bottom 96 well-plate (Costar) and the ThT dye was added to a final volume of 260 µL and contents of each well were mixed by pipetting. These, along with suitable control wells corrected to volume with no sample added to the ThT solutions, were read on a SPECTRAmax® GEMINI XS dual-scanning microplate spectrofluorometer with excitation set to 450 nm and emission set to 482 nm.

Time course analysis of amyloid increase within a sample was performed using a single solution and removing aliquots for analysis over a time series. This option was employed in order to reduce the variability that is inherent in time series samples that are taken from a series of samples started separately. Thus, for each replicate of a time course series, data were obtained by serially sampling a single solution. Multiple samples were processed in this way in parallel when experiments were performed. At the beginning of an amyloid time course (time 0), for a reaction tube containing 100 µM MES, 1 mM SDS, and 1mg/mL αS was prepared for each type of treatment; which included untreated, extract fraction 5A treated and extract fraction 5B treated. For each treatment; the concentrations of MES, SDS and αS were the same and an extract fraction was added at the most effective concentration, 4 $mg \cdot mL^{-1}$. After mixing, two 20 µL aliquots were removed for time 0 and frozen. At this point the reaction was carried out exactly as before, with repeated removal of aliquots from a single reaction tube per treatment. ThT was

added to each well as before, and fluorescence read with excitation set to 450 nm and emission set to 482 nm. The second set of 20 µL aliquots was reserved for TEM and CD follow-up experiments.

A similar fluorescence assay to ThT was reported to allow reporting on monomer and aggregate populations of amyloid using the dye JC-1(Lee et al. 2009). The dye used was tested at concentrations ranging from 0.1 to 0.5 and the concentration of αS used ranged from 0.1 to 0.5mg·mL^{-1}. The excitation wavelength was set to 490 nm and the emission was measured as a spectrum from 500nm to 600nm. Ideally a monomer peak would appear at ~520nm and a multimer peak at ~580nm.

2.4 SDS-PAGE

The SDS-PAGE was carried out according to standard procedures (Laemmli 1970). A 15% acrylamide separating gel was selected for use with αS in order to allow resolution of this 14 kDa protein. The final concentrations of the lower buffer were 1.50 M Tris-HCl, and 0.5% SDS w/v, mixed to pH 8.8; and the final concentrations of the upper gel buffer were 0.5 M Tris-HCl and 0.5% SDS w/v, mixed to pH 6.8. For the 10X SDS-PAGE running buffer, components were mixed to 0.25 M Tris-HCl, 1.92 M glycine, and 35 mM SDS.

The Pageruler Prestained Protein Ladder (Thermo Scientific) was run alongside the samples on the gel in order to determine relative sizes of protein from the migration of the bands. A BioRad Mini-PROTEAN II gel dock was set to 200 V and run until the indicator dye in the sample buffer

reached the end of the gel. The gel was then stained with GelCode Blue (Thermo Scientific) Coomassie Blue stain, according to the protocol supplied with the product. The gel was washed three times with deionized water over a period of 15 minutes, and then it was immersed in GelCode Blue stain for one hour. A further wash in deionized water was performed if needed following staining.

2.5 Transmission Electron Microscopy

In order to confirm the development of amyloid fibers in the ThT experiments and to detect any differences in amyloid with the addition of algal extract, samples of the αS used in the ThT experiment were examined by transmission electron microscopy (TEM). The microscopy was completed with the assistance of Cindy Leggadrio and Dave O'Neil at NRC.

In a fume hood, 10 µL drops of the samples were pipetted onto a Parafilm surface. A carbon coated copper TEM grid (Canemco, St. Laurent, Quebec) was placed carefully on the surface of each drop using forceps and allowed to rest on drop for 5 minutes, removed and allowed to dry for 10 minutes. The grids were then moved to wells containing 45 µm syringe-filtered 2% uranyl acetate, pH 4.0 using an inoculating loop, and allowed to sit for approximately 5 minutes in relative darkness. All grids were then washed 4 times by floating on a series of clean drops of 45 µm syringe-filtered distilled water for approximately 1 minute each. Grids were then dried gently by touching them to the edge of a filter paper (Whatman) and allowing them to air dry, suspended by the forceps for approximately 10 minutes. Sample grids were then viewed by TEM.

A series of photos were taken across the range of the grid and then further photos taken in regions where fibrils were evident. For some of the latter pictures, the focus was adjusted to the plane just above the fibril surface and then to the plane just below the fibril layer to allow further visualization of heavily tangled regions. These regions looked like clumps initially, but using different focus on the same area showed they were knots of fibril. Photos were taken at magnifications ranging from 20 000 – 100 000X.

2.6 Circular Dichroism

Circular dichroism (CD) experiments were undertaken to examine the secondary structure of αS and the effect the algal extracts had on it. It is known that secondary structure features, such as α helices and β sheets exhibit characteristic CD spectra. Through comparison to proteins known to have given structures as determined by X-ray crystallography, one can make estimations about the structure of an unknown protein (Greenfield 2006). Measurements were made using a Jasco- J810 device at Dalhousie University. The CD analysis was carried out as described by Greenfield et al in 1969 (Greenfield and Fasman 1969). Samples were run for each type of treatment from the thermal shift, as well as a buffer run for each. The samples were placed in a 0.2 mm path lenth quartz cuvette and data was collected 3 times, over the wavelength range of 190-260 nm and averaged. In addition, the buffer, which was 10 mM MES pH 6 with 1 mM SDS, was run as a control using the same parameters. The samples included samples taken

from the beginning and end of an incubation in the presence and absence of algal extract fractions 5, 5A and 5B.

Accurate αS concentration values are needed to calculate mean residue ellipticity from CD data, so this was determined by measuring absorbance at 275 nm and determining the αS concentration from that value, based upon its extinction coefficient at 275 of 5600 M^{-1} cm^{-1} (Shvadchak et al. 2011). Duplicate readings were taken from each CD sample and the mean value was used.

Since most secondary structure prediction methods based upon CD spectra require data for wavelengths below 200 nm, the data obtained in MES could not be used as the buffer interferes with the data integrity in the 190-200 nm region. Therefore, a method of analysis requiring specific elipticity values above 200 nm was used (Greenfield and Fasman 1969). Employing this method, the % α helix could be estimated by the equation:

% α helix = (molar ellipticity at 208 nm) – 4000)/(33000-4000)

The proportions of β sheet and random coil structure could be estimated from the values obtained at 217 and 222 nm, respectively, according to this method.

CHAPTER 3: RESULTS

3.1 Optimization of the Thermal Shift Assay

3.1.1 Implementation and Assessment of the Thermal Shift Assay

Over the course of the study, conditions for thermal shift determination were optimized. The analyses shown in Figure 5 were obtained using a more rapid temperature ramp and slightly different protein preparation conditions from the analyses that followed, as described in the Materials and Methods. The enzyme carbonic anhydrase has previously shown a predictable thermal shift upon binding the inhibitor TFMSA (Matulis et al. 2005). Therefore, this enzyme was used during the set up and optimization of the thermal shift assay for this project. Early experiments resulted in clear T_m values, but with a high level of variability (not shown). Using the Roche thermal cycler, the ramp speed was not adjustable and the default speed was far more rapid than the rate of temperature change used in experiments described by others such as (Matulis et al. 2005). Therefore, the ramp speed was diminished by adjusting a related parameter, the number of temperature acquisitions per °C. By increasing the number of acquisitions per °C from 10 to 70, the total ramp time for the 25°C to 85° temperature interval increased from 10 minutes to one hour. Concentrations of TFMSA used ranged from 0 to 100 μM. These conditions allowed a clear measurement of a change in the melting point of CA, with an increase in the T_m of 8.4 °C ± 2.08 with 100 μM of TFMSA. A one way ANOVA, using a Dunnett's post test, with the control mean set at 0μM TFMSA, showed that the difference in T_m

was significant at 10 μM TFMSA and above, up to the max concentration used, 100 μM TFMSA. The results of the TFMSA experiment are shown in Figure 6.

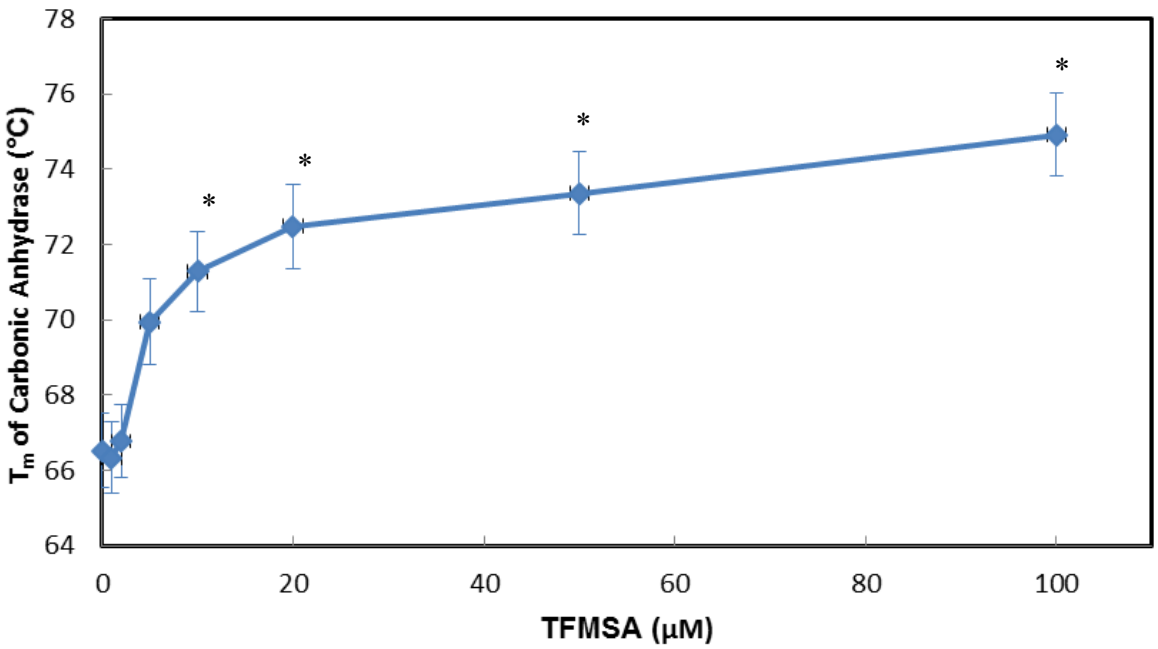

Figure 6: Thermal shift analysis using carbonic anhydrase as a model protein. The mean T_m values for carbonic anhydrase were determined as a function of TFMSA concentration as described in the Materials and Methods. Data shown are the means ± SEM. The error bars display standard error of the mean for each concentration of TFMSA. All data points above and including 10 µM TFMSA were found to be significantly different from carbonic anhydrase alone by one way ANOVA Dunnett's post-test as indicated by *.

3.1.2 Detergent and Buffer Optimization

The TMAO did not affect the T_m of αS in the HEPES pH 7.4 and the 1mM BOGS, but it did affect the T_m of the αS in the MES pH 6.0 and 1mM SDS. There was an observable, TMAO concentration dependent effect on the T_m of αS in MES and SDS; 62.5 mM TMAO caused a 3.38°C shift, 125 mM TMAO caused a 4.04°C shift; 250 mM TMAO caused a 7.84 °C shift; and 375 mM TMAO did not produce a discernable peak. The T_m of αS is plotted against concentration of TMAO in figure 7.

It was determined that 1mM SDS with MES as the buffer and 1mM BOGS with HEPES both produced repeatable peaks assumed to be the point of secondary structure unfolding. Additionally, both SDS and BOGS were added to αS in MES buffer and two distinct peaks, both characteristic of one detergent, were observed.

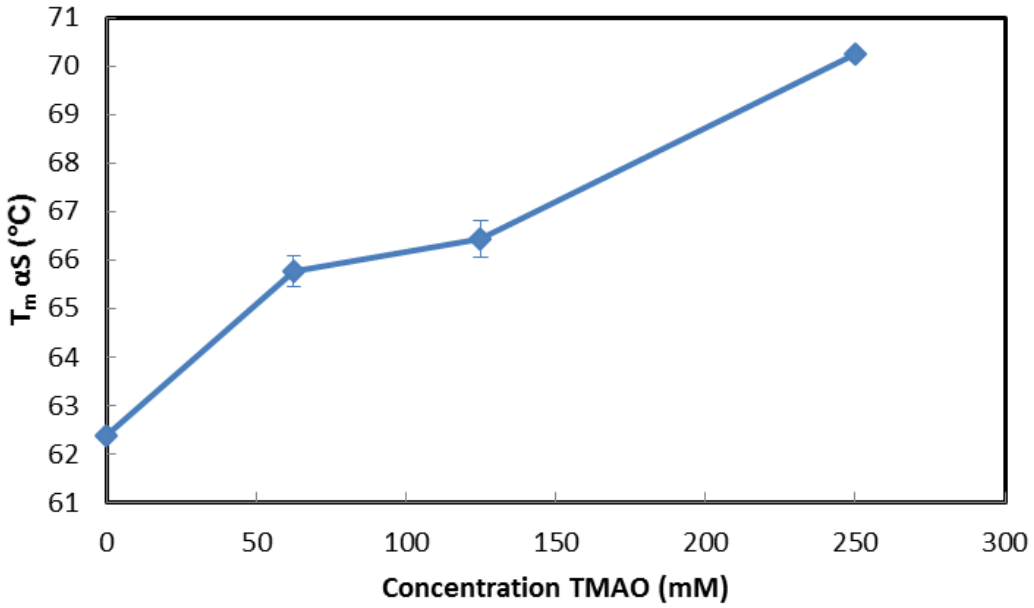

Figure 7: Variation in T_m of αS with TMAO concentration. The αS was treated with varying concentrations of TMAO as described in the Materials and Methods. The error bars display standard error of the mean for each concentration of TMAO.

3.1.3 Effect of Algal Extracts on the Melting Temperature of αS

Extract 5 was re-evaluated using the optimized conditions, which were the following: 1 hour temperature ramp time (25°C - 85°C); freshly thawed αS at 0.1 mg/mL; 0.1 M MES buffer pH 6.0 containing 1mM SDS detergent and 1x SYPRO Orange dye. The reaction volume was 20 µL and various concentrations of extract ranging from 0 – 1000ug/mL were evaluated. A representative thermal shift is displayed in figure 8, with the negative derivative of fluorescence plotted against temperature. The point taken to be the T_m is the point of greatest change in fluorescence, in other words when the most hydrophobic resiudes are exposed at once. On the negative derivative of fluorescence graph this is where the value is most diminished. The results were significant this time; over 5 separate experiements each with duplicate wells. The minimum and maximum changes were a 5.07 ± 1.61 °C shift down at 0.05 mg/mL and a 9.26 ± 0.91 °C shift up at 1 mg/mL. The difference in T_m for each concentration is plotted in figure 9.

A concern with the use of protein thermal shift is that any protein in the extracts being tested could contribute to the shift or create noise in the data. Although the extracts were prepared in a manner to exclude protein, experiments were conducted using extracts treated to remove any possible residual protein. Extract 5 was subjected to acetone precipitation and to pepsin digestion. The activity of the pepsin was confirmed by its digestion of carbonic anhydriase II followed by SDS-PAGE analysis in figure 10. As the intact protein present in both the undigested BSA was completely destroyed by pepsin, the enzyme was confirmed as active. The Pageruler Prestained Protein Ladder was used in an SDS – PAGE gel made in the same way as the 15% gel above, with three adjacent wells containing; boiled 0.0138mM αS in reducing

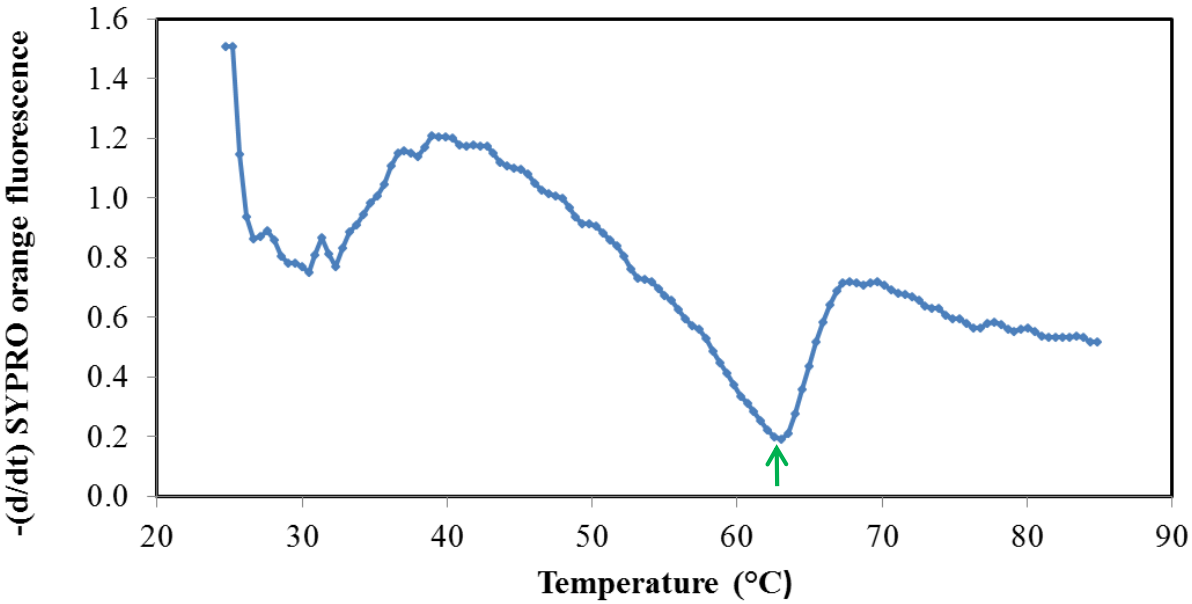

Figure 8: Representative change in SYPRO orange fluorescence with temperature in the presence of αS. The graph (blue) shows the negative derivative of SYPRO orange fluorescence. SYPRO orange is quenched in an aqueous environment. So, as a protein unfolds and exposes hydrophobic regions that shield it, SYPRO orange fluorescence increases. The region in the graph where the most rapid change in fluorescence is indicated by a minimum in the graph, which corresponds to the T_m of the protein (green arrow).

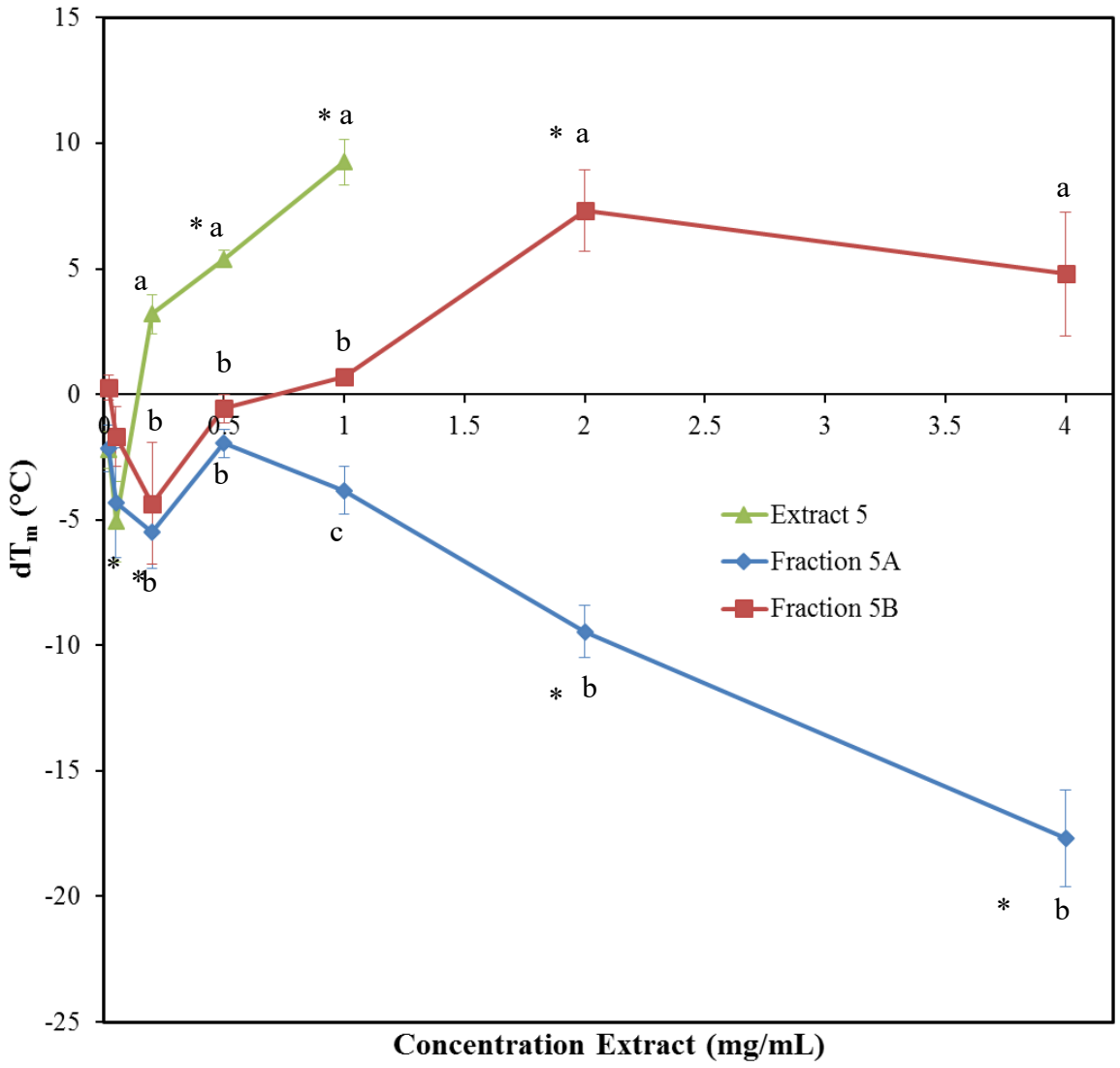

Figure 9: The change in melting temperature (T_m) of αS, as observed by SYPRO orange fluorescence as a function of the concentration of marine Extract 5 and of two extract fractions, 5A and 5B. Means different from the untreated protein (ANOVA with Dunnett's test, $p<0.05$) are indicated by an asterisk; means that differ among extracts at a given treatment concentration are indicated by letters (T test, $p<0.05$).

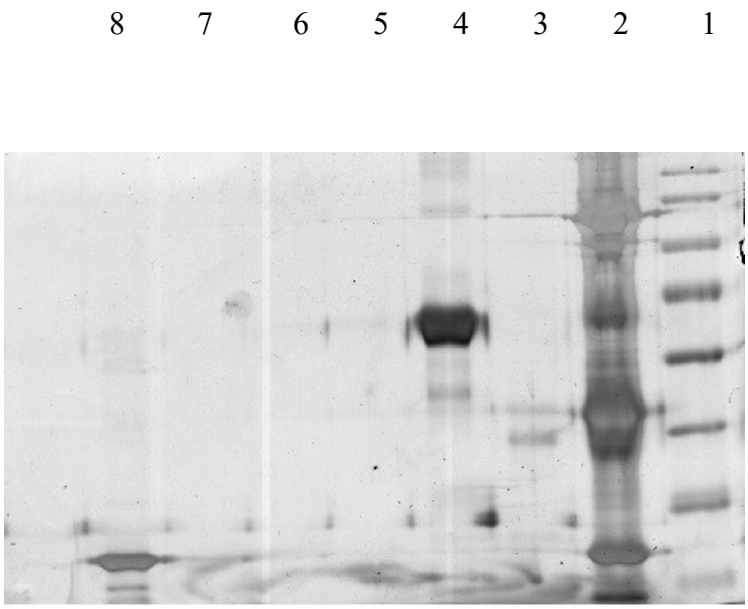

Figure 10: SDS PAGE analysis of pepsin enzymatic activity. The products of pepsin digest were compared to their undigested original proteins. PageRuler prestained protein ladder used in lane 1, labeled by size in kDa. Contents of the other lanes are as follows: 2 digested protein ladder; 3 digested BSA; 4 undigested BSA (actual MW known to be 66.5 kDa); 5 – digested extract 5; 6 undigested extract 5; 7 digested carbonic anhydrase; 8 undigested carbonic anhydrase

conditions (BME); 13.8 μM αS and a 20 fold molar excess of BS^3 (276 μM); 13.8 μM αS and a 50 fold molar excess of BS^3 (552 μM). The results of this are not shown, as no multimers as described in Bartels were observed.

The effect of pepsin digestion of Extract 5 on its activity in the thermal shift of αS was examined along with that of a control-treated extract, showing a 7.38 ± 0.44 °C change in the thermal shift (Figure 11). This was found to be not significantly different from the thermal shift of untreated extract 5 (both at same concentration 1 mg/mL) by ANOVA with Dunnett's post test.

The results with the acetone-soluble and acetone-insoluble extract fractions were more complex. Compared with the untreated control, the soluble (supernatant) portion. The extract preparations treated with pepsin with acetones-soluble and insoluble and supernatant of extract 5 were both used in the αS thermal shift experiment and upon analysis of the results it was noticed that the down shift in T_m was present in the pellet and the shift up was present in the supernatant (both at 1 mg/mL). For the acetone precipitation, two thermal shift experiements were carried out on samples of Extract 5 that had been precipitated using a standard protocol, and then two more were carried out using the products of an acetone precipitation using glass-distilled acetone and presoaked tubes to rule out any contamination. The results were averaged over all experiments and the pellet caused the T_m of αS to shift down 6.2 ± 0.8 °C and the supernatant caused it to shift up 9.6 ± 0.5 °C. The opposite effects of the acetone insoluble and acetone-soluble materials suggested that distinct components of the extract were acting in different manners on the Tm. These results are displayed in figure 11.

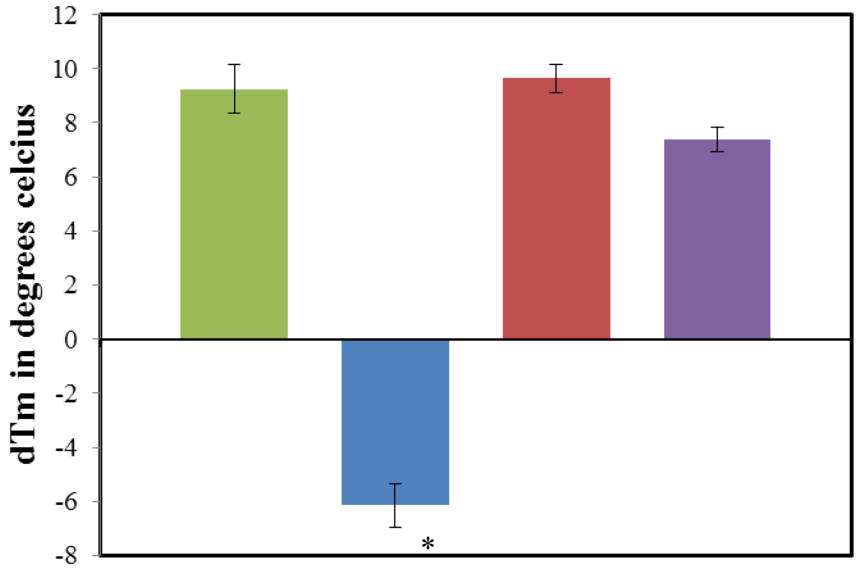

Figure 11: Effect of chemical and enzymatic treatments on activity of Extract 5 in modulation of αS T_m. The change in T_m of Extract 5 without treatments, in the presence of an acetone-insoluble fraction of Extract 5; in the presence of acetone-soluble material from Extract 5 and the product of a pepsin digest of Extract 5. Bar colours are green for the untreated extract, blue for the acetone pellet from extract, red for the acetone supernatant from extract and violet for the pepsin-digested extract. Each bar represents the change in T_m of αS in the presence of extract 5 treated in various ways. Means different from the untreated extract (ANOVA with Dunnett's test, $p<0.05$) are indicated by an asterisk.

Once it was established that there were two separate activities, size fractionation of the extract was attempted to see if they could be further characterized. The result was that the positive and negative T_m shift could be separated by size: fraction 5A (5-10 kDa) caused a drop in T_m and 5B (10 kDa and above) caused an increase in T_m. Extract fraction 5A caused a 17.7 ± 1.9 °C T_m shift downwards and extract fraction 5B caused a 7.3 ±1.6 °C T_m shift upwards. The thermal shift experiments completed with fractions were performed three times each with duplicate wells in each experiment. The results of the extract fraction thermal shift experiments are graphed in figures 9.

One way ANOVA analysis of the results from the thermal shift experiments are displayed in figure 9. For the whole extract, concentrations 0.5 mg/mL and 1mg/mL were shown to be significantly different from untreated αS; extract fraction 5B was significantly different from untreated αS at a concentration of 2 mg/mL; and extract 5A was significantly different from untreated αS at 0.2 mg/mL, 2 mg/mL, and 4 mg/mL. T-tests were also performed to test if extracts were different from each other at a given concentration. The results of these t-tests are also displayed in figure 9, with letters identifying means not shown to be significantly different from each other.

3.2 ThT Assay for Amyloid Detection

Initial ThT assays were carried out as each experiment consisting of 5 tubes containing 0.1 mg/mL αS in MES buffer with SDS detergen, as described above. These did not produce repeatable fluorescence results. Since this did not work, a new approach focusing on better

conditions for a single nucleation were considered. The concentration of αS was increased tenfold to 1 mg/mL and the experiment carried out in one tube for each treatment, rather than one for each measurement. Using this method, the results obtained were repeatable; any untreated αS would be expected to have a significant increase in ThT fluorescence by 48 hours and onwards, which was observed, and neither extract 5A treated or 5B treated αS produced significant increase in ThT fluorescence in any instance.

The results of at least three separate 144-hour experiments with duplicate wells for each type of treatment as well as untreated αS are displayed in figure 12. Incubated buffer was used as a blank by subtracting its ThT fluorescence at 482 nm from all other readings. Detailed results are outlined in tables displayed in figure [#]. The change for untreated was 388 ± 62, the change for 5A treated was 139 ± 43, and the change for 5B treated was 113 ± 71. Within treatments, the one-way ANOVA with Dunnett's post-test revealed that only untreated αS showed a significant increase in ThT, and only at 48 hours, 72 hours, and 144 hours of incubation. Differences among treatments at specific time points were examined using T-tests; these were only different after144 hours of incubation (Figure 12).

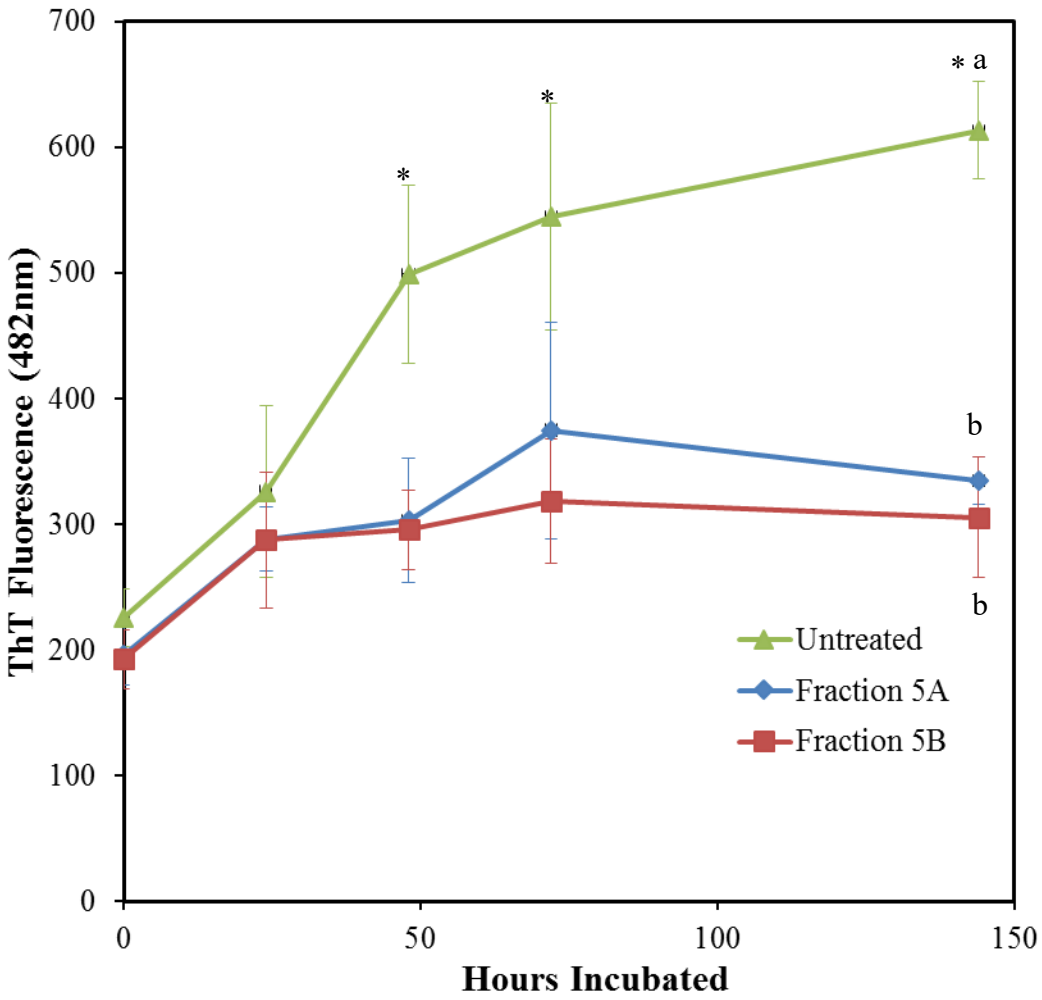

Figure 12: Thioflavin T (ThT) fluorescence over time in the presence of αS in the presence and absence of algal extract fractions. The effects of the two fractions of Extract 5, Fractions 5A and 5B, were determined. Measurements were taken over a time course at 37ºC with 200 rpm shaking. Samples of AS were incubated at 1mg/mL in 0.1 M MES and 1mM SDS in a heated orbital shaker. Means different from time 0 reading (ANOVA with Dunnett's test, $p<0.05$) are indicated by an asterisk; means that differ among extracts at a given treatment concentration are indicated by letters (T test, $p<0.05$). Both fractions 5A and 5B prevented the increase in ThT fluorescence over time.

3.3 Transmission Electron Microscopy of Amyloid Fibers

Samples removed from the ThT assay were stained with uranyl acetate and observed at 20,000X, 50,000X and 100,000X magnifications with a TEM. Fibers were observed, but only in untreated samples of αS after suitable incubation times. For each condition (untreated, 5A-treated, 5B-treated, and buffer control) two grids were prepared for time 0 and time 144 hours. Three random images were taken from each, and then additional images were taken of any visible fibers or other objects present. It was found that extract fraction 5B contained small dark spherical objects that were not observed in fraction 5A. Controls with no protein corroborated the presence of the small globules in fraction 5B, and absence of globules in fraction 5A. The fibers observed on the untreated αS grid were abundant, and exhibited a tube-like morphology as seen in several previous studies (Conway, Harper, Lansbury 1998) when the image was overfocused. What is meant by this is the TEM is focused normally looking down on the fibers and then the fine know is adjusted to focus on the bottom of the fiber rather than the top. An interesting insight gained from this was the nodules observed turned out to be folds or "knots". A sheet of representative TEM images is displayed in figure 13, as well as some examples of the overfocused pictures in figure 14.

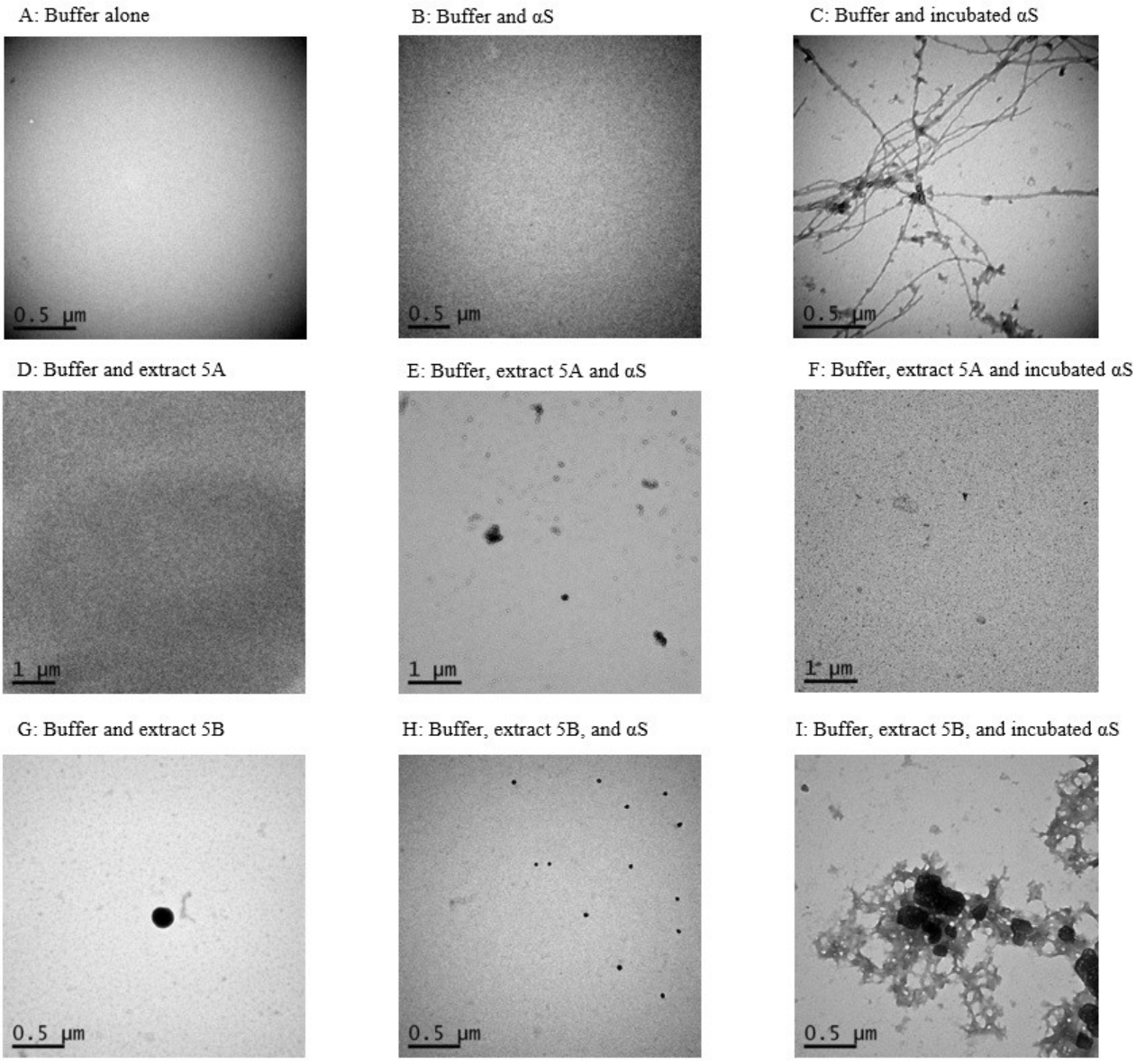

Figure 13: TEM images taken of incubated αS samples stained with uranyl acetate. Panels A-C contain no extract; A is buffer alone, B is buffer and protein, and C is buffer with incubated protein. D-F contain extract fraction 5A; D is buffer and extract; E is buffer, extract and protein; and F is buffer, extract and incubated protein. Images G-I contain extract fraction 5B; G is buffer and extract; H is buffer, extract and protein; and I is buffer, extract and incubated protein.

αS 144 Hours Incubated normal focus

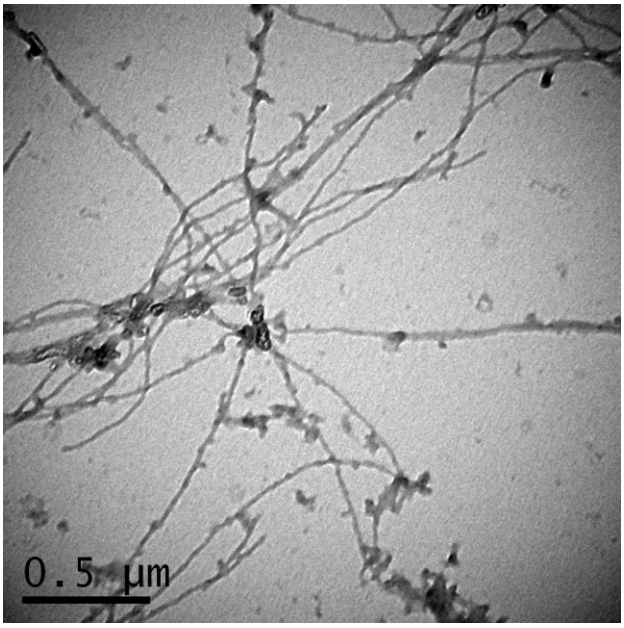

“Overfocused” the same view to reveal nodules as “knot” structures

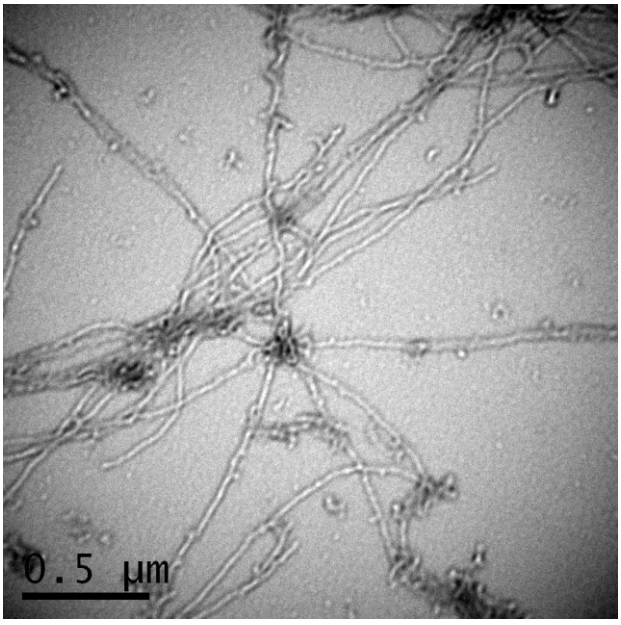

Figure 14: Untreated αS 144 Hours Incubated; Image on top is in focus and bottom image is overfocused, revealing possible “knots” in fibers. Magnification 50 000x.

3.4 Circular Dichroism for Secondary Structure of αS

Aliquots reserved from ThT experiment were also used to examine the conformation of the αS protein. Each CD spectrum obtained was corrected for concentration of protein, as determined by a photometer and the elimination constant for αS at 280 nm. These spectra were then analyzed using the method described by Greenfield (Greenfield and Fasman 1969). As expected in the presence of SDS, αS protein showed minima at 208 and 222 nm consistent with α-helix content. It was determined that the helical contents of the αS at time 0 for untreated, 5A treated and 5B treated αS were 32%, 30% and 27 % respectively as shown in figures 15-17. After incubation with the extracts, the helical contents dropped to 22%, 20% and 19% respectively as shown in figures 15-17. A reduction in α-helix content was observed in all samples after incubation, treated and untreated. This suggests that the structure that was observed (and melted) in the thermal shift assay was native α-helix. Comparisons of the three treatments at time 0 are shown in figure 18 and at time 144 figure 19.

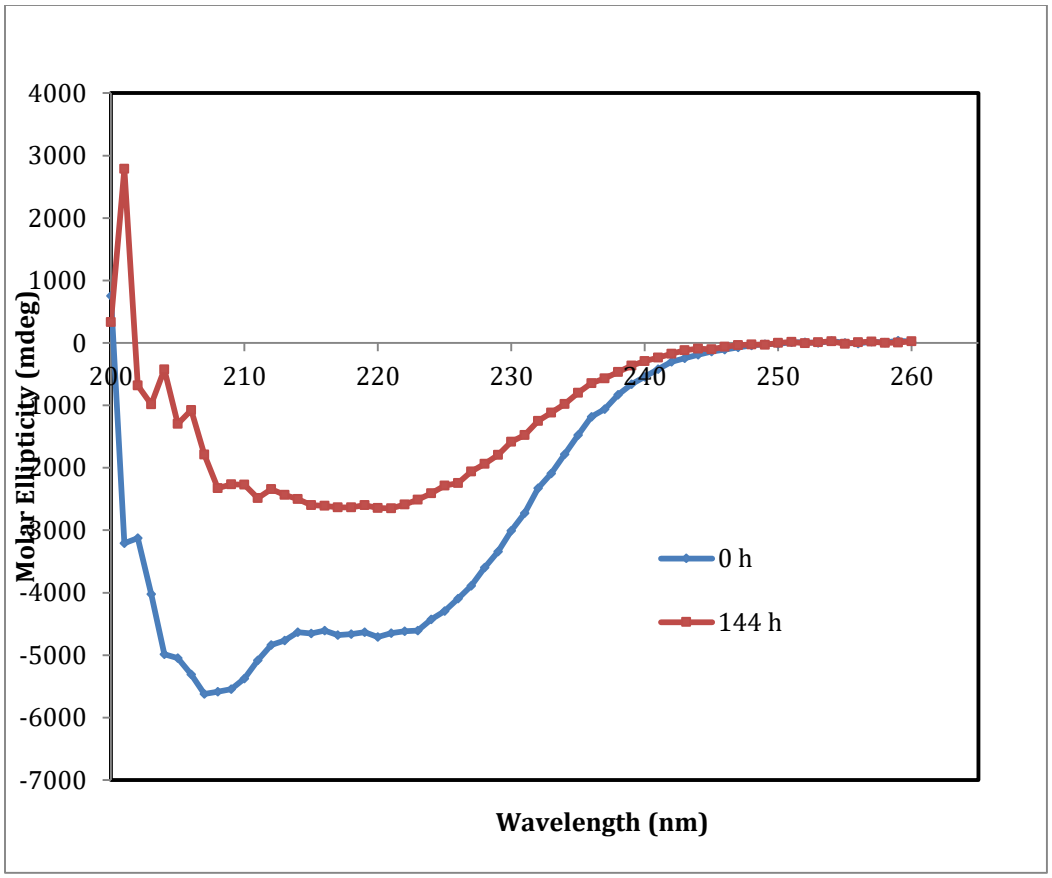

Figure 15: Circular dichroism analysis of the αS in the solution used in the ThT assay. The protein was predicted to have 32% α-helix content using the method described by N. Greenfield (1969).

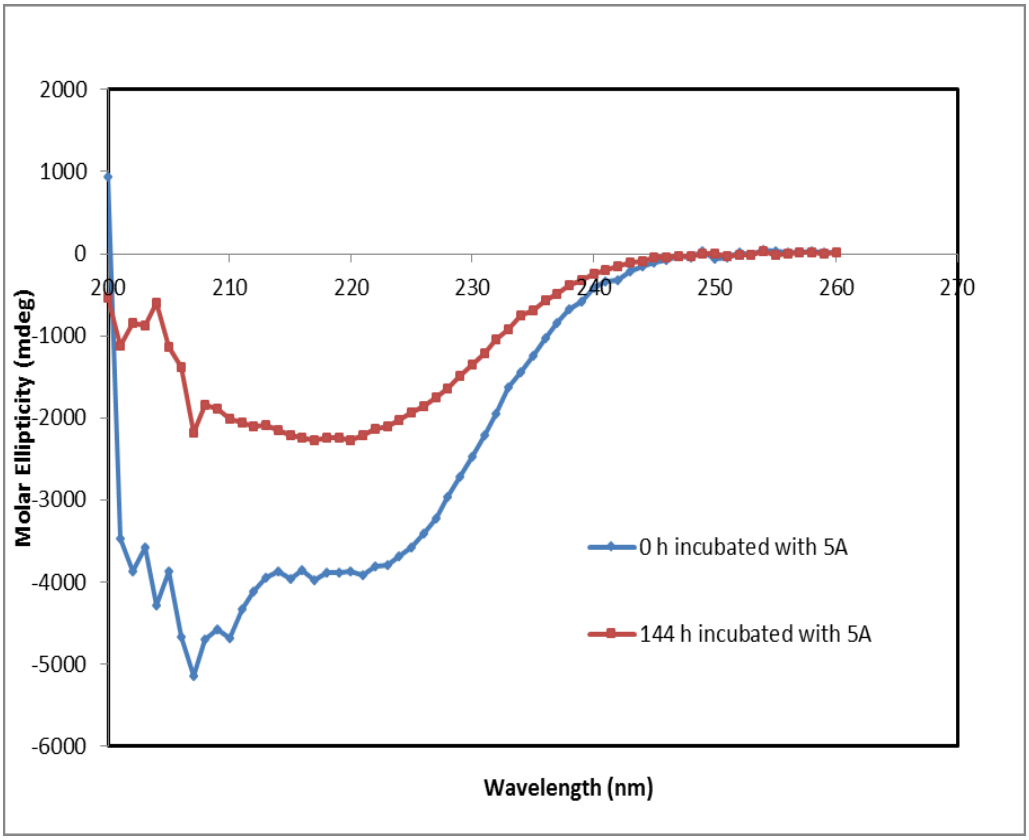

Figure 16: Circular dichroism analysis of the αS in the solution used in the ThT assay. This is a comparison between αS treated with 5A and αS treated with 5A after 144 hours incubation. The protein with fraction 5A was predicted to have 30% α-helix content using the method described by N. Greenfield (1969).

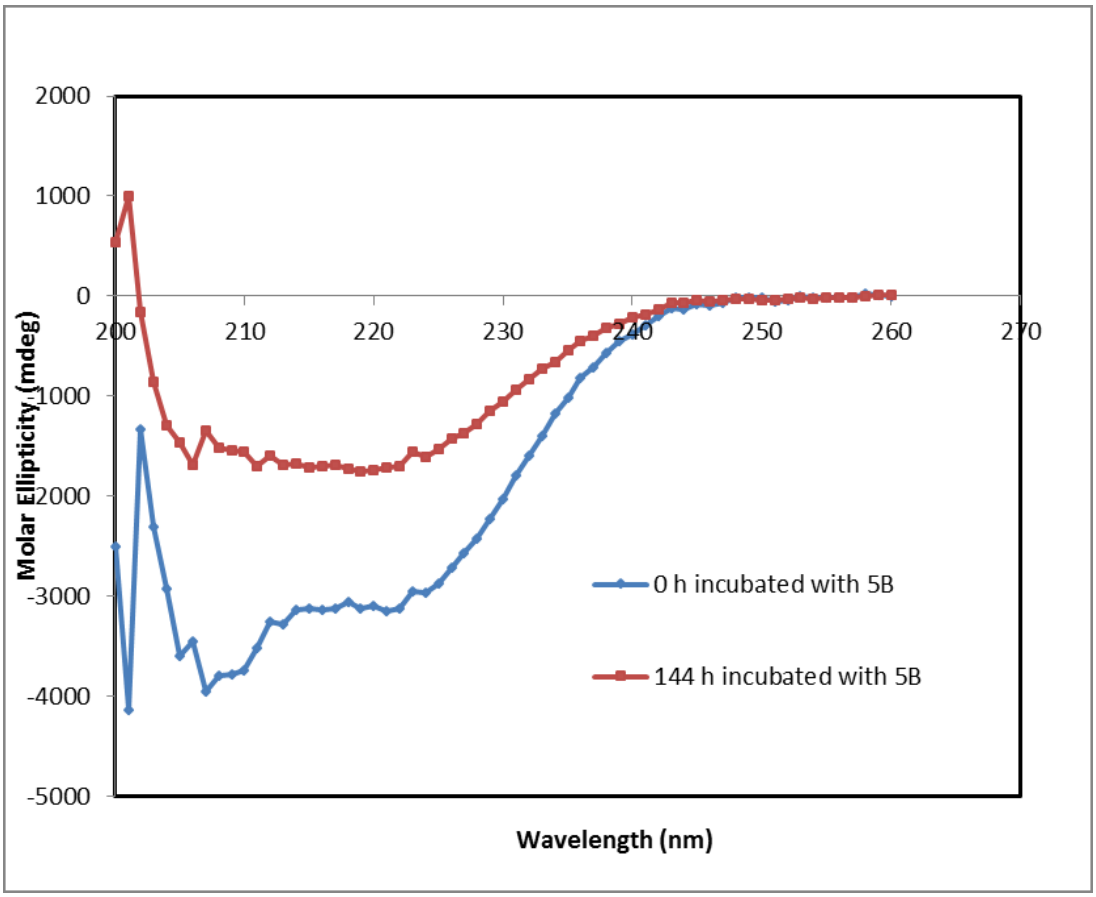

Figure 17: Circular dichroism analysis of the αS in the solution used in the ThT assay. This is a comparison between αS treated with 5B and αS treated with 5B after 144 hours incubation. The protein with fraction 5B was predicted to have 27% α-helix content using the method described by N. Greenfield (1969).

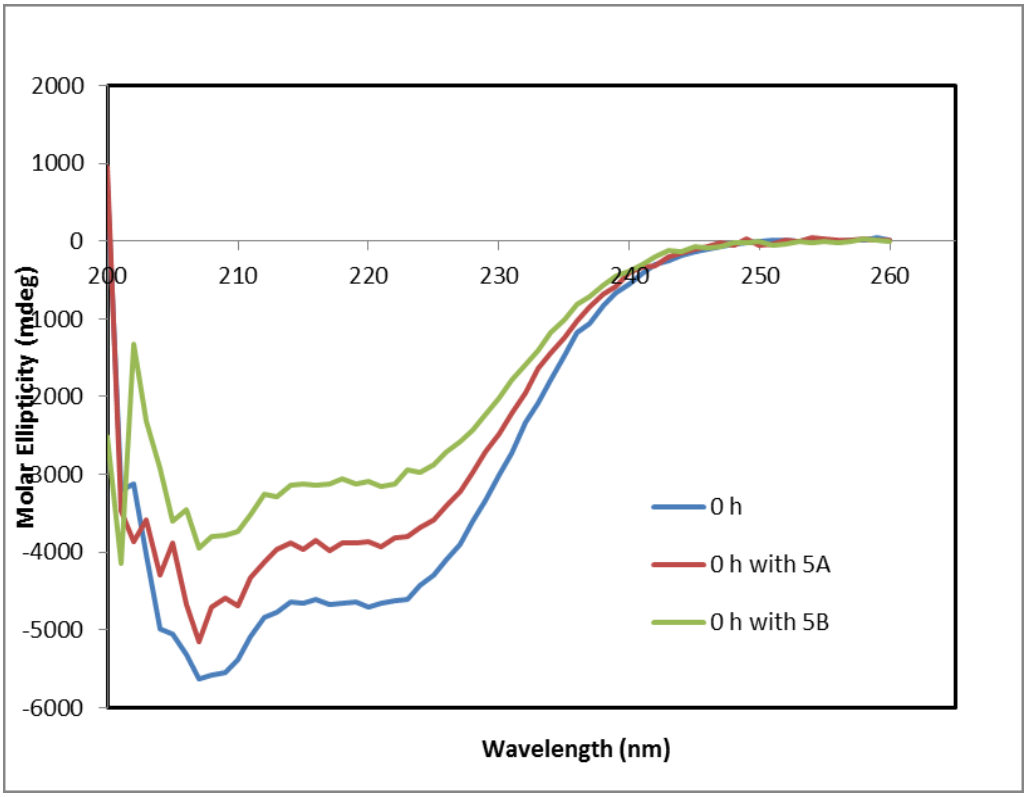

Figure 18: Circular dichroism analysis of the αS in the solution used in the ThT assay. This is a comparison between untreated αS and αS treated with 5A or 5B before incubation.

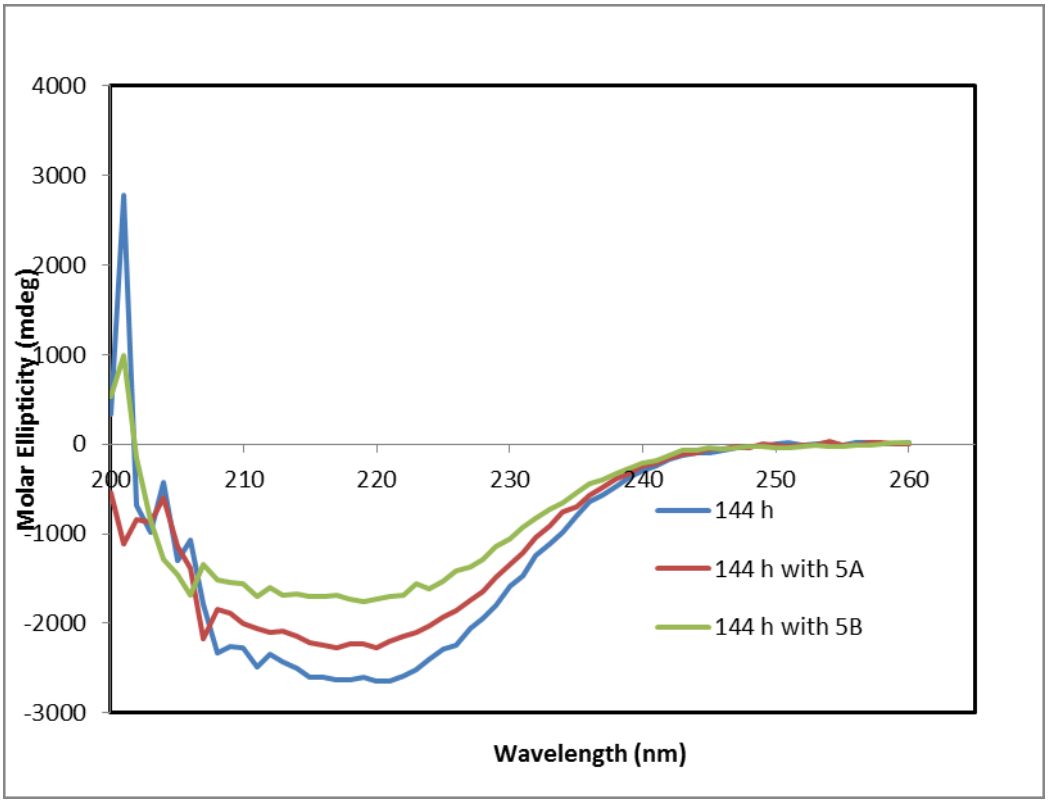

Figure 19: Circular dichroism analysis of the αS in the solution used in the ThT assay. This is a comparison between untreated αS and αS treated with 5A or 5B after 144 hours incubation.

CHAPTER 4: GENERAL DISCUSSION

4.1 Modulation of αS Fold Stability

In its native form αS forms α helical tetramers or unfolded monomers (Bartels et al., 2011). The tetrameric form is resistant to amyloid fibril formation because it would most likely have to unfold before forming the predominantly β sheet structures in amyloid oligomers and fibrils. In agreement with this, an increase in the ratio of monomers to tetramers appears to initiate pathogenesis (Dettmer et al., 2015). Therefore a possible option to prevent Parkinson's disease development is to maintain the stable folding of tetrameric α helical αS. The complete algal extract from *A. esculenta* significantly reduced the thermal stability of αS at low concentrations, whereas higher concentrations of the complete extract increased the stability. This prompted a fractionation of the algal extract, with fractions produced by filtration that were greater than 10 kDa and that were smaller than 5 kDa. Evaluation of these fractions in a thermal shift assay revealed divergent effects on αS fold stability, as extract 5A lowered the melting temperature of folded αS, whereas 5B raised the melting temperature. Together, these results indicated the presence of components within Extract 5 with divergent effects on αS.

The thermal shift assay which was used to identify components 5A and 5B offers a convenient and informative platform for initial assessment of protein folding stability. The thermal shift assay is cost-effective and highly sensitive, making it an idea screening method for the discovery of novel molecular chaperone activities (reviewed by Huynh and Partch et al.,

2015). Some setup can be required in order to ensure that a particular thermal cycler allows assay parameters and sample detection that are appropriate for the assay. Nonetheless, in the case of αS, a few experiments using carbonic anhydrase as a test protein and then αS itself provided the initial data required for assay optimization. One condition of using a thermal shift assay is that the protein of interest must have a folded state to detect and it must be one that binds the indicator dye, SYPRO Orange. With αS, and other proteins that exist partly or exclusively in a natively disordered configuration, a melting point can only be detected if a folded state can be induced. In the case of αS, the addition of a submicellar concentration of SDS (1 mM) was sufficient to favour a folded form. The thermal shift does not distinguish between these alternative folds. For this reason, shift data for proteins with partially or fully unfolded character must be interpreted with caution.

Another limitation of thermal shift data using a complex extract was that there was a small risk that the extract contains protein, which might fold and bind SYPRO Orange. Other moderately sized molecules could have done so as well. Because extract run in a thermal shift assay showed no apparent SYPRO Orange-binding structure or melting thereof (preliminary data), this could be attributed to the αS alone; however, in order to be certain of that, the extract was acetone precipitated and also digested with pepsin to remove any possible protein and thermal shift assays were repeated. Since the acetone-soluble and pepsin-treated extract showed the same thermal shifts as the untreated extract, it was clear that exogenous protein was not a factor in the positive thermal shift of αS by the extract.

4.2 Modulation of αS Amyloid Fibril Formation

Since conversion of αS to its amyloid form appears to be the key process in the development of Parkinson's disease (Uversky and Eliezer, 2012; Luk et al., 2012), the effects of algal extract fractions on amyloid formation were examined *in vitro*. The formation of amyloid fibrils by αS is typically carried out over several days with rapid shaking after which binding of ThT is diagnostic of amyloid formation (LeVine et al., 1999). Under the conditions used here, 1 mg/mL of αS was required in order to generate reproducible ThT binding indicative of αS aggregation. Furthermore, maximal signal required 6 days of incubation. Thus, although the measurement of amyloid formation was ideal for the purpose of this study, the formation of amyloid requires substantial protein concentrations and time investment in order to generate reliable results detectable by ThT binding.

The six-day incubation of αS with agitation resulted in a significant increase in ThT fluorescence, indicative of amyloid fibril formation, whereas no significant increase in fluorescence occurred in the presence of algal extract fractions 5A or 5B. Both fractions 5A and 5B, which respectively had decreased and increased the T_m of αS, inhibited fibril formation in this assay. However, the TEM images of the incubated products revealed qualitative differences in the effects of the two fractions, as 5A generated no observable aggregates and the 5B generated aggregates that appeared distinct from the elongated fibrils visible in the untreated samples. There appear to be a few folding alternatives, in which an amyloid-forming protein may have different stabilities and resulting T_m values while being off the fibril-forming pathway (Fig. 4). Such a scenario may explain the differences between the αS melting point and fibril

formation results obtained in the presence of the extract fractions. Alternative non-amyloid aggregation was suggested previously for aβ (McLaurin et al. 2000). The non-amyloid aβ aggregates did not have the same toxic effects as amyloid aggregates on primary human neuronal in culture (McLaurin et al. 2000). Consistent with those findings, EGCG was found to direct aβ and αS aggregates into alternative non-toxic forms (Ehrnhoefer et al., 2008). This is a promising possibility for the prevention of PD. A compound that diverts αS association toward the formation of globular aggregates, instead of amyloid oligomers and fibrils, may reduce cytotoxicity.

4.3 Secondary Structure of Treated and Untreated αS

Under physiological conditions, αS protein is known to exist both in an α-helical folded conformation and in an extended, natively unfolded, structure (Bartels et al., 2012; Fonseca-Ornelas et al., 2014), whereas amyloid fibrils are composed of β-sheet. Therefore, analysis of the secondary structure composition of αS offered unique insight into the folded structure of the protein under the conditions used in this study and in response to algal fraction addition. In order for the CD spectra to be directly informative in this study, the αS solutions that were analyzed were taken directly from the ThT assays. The buffer MES was used in the ThT assay, and MES did not allow reliable data collection at wavelengths below 200 nm. The absence of lower wavelength data precluded reliable deconvolution of the spectra to determine the relative contents of random coil (unstructured), α-helix and β-sheet; however, qualitative analyses of the spectra were directly informative and, by using a method relying on data collected at higher wavelengths, the α-helix percentage in the protein was predicted.

All spectra for αS collected prior to incubation showed a clear minimum at 208 and a slighter one at 222 mm, each of which is diagnostic of substantial α-helical content and calculated helical contents ranged from 27 to 32%. This result is consistent with the structure reported for αS in the presence of SDS (Rivers et al., 2008; Bazak et al., 2014). In contrast, spectra collected following the ThT experiment incubation exhibited lower intensity and appeared most consistent with a minimum at 218 nm, which occurs in the presence of β-sheet. Calculated helical contents of these spectra were lower, ranging from 19-22%. Although the intensity of the spectra differed among the untreated sample and those treated with extract fractions 5A and B, they changed in the same manner with incubation. The fractions do not appear to alter the α-helix propensity of the starting material, nor do they affect the apparent shift toward β-sheet in soluble protein over the course of incubation. This suggests that the extract fractions reduce amyloid fibril formation by preventing aggregation of αS at a point after its transition to β-sheet in solution.

4.4 Future Research

A number of interesting results obtained in this project warrant further investigation. Identification of the active components of each extract fraction may more clearly indicated how they act on αS. Identification of the active components would allow direct assessment of each species and location for the component as a means of to determine if it is a practical source of the component. Furthermore, once a component is identified, testing in cellular studies would be the next logical step in the path toward determining potential as a treatment for PD *in vivo*. Finally, tests in animal models would be informative. For example, a fraction from another local

seaweed was tested in a transgenic *Caenorhabditis elegans* worm model of PD that expresses human αS (Liu et al., 2015) and a blueberry extract was evaluated in an analogous transgenic Drosophila model (Lipsett and Staveley, 2014). Using whole-animal models allows insight into the availability and behaviour of a compound *in vivo*, allowing decisions on further study directions to be made.

4.5 Concluding Remarks

The north Atlantic is an untapped resource in terms of organisms that have adapted to live in extreme environments with variations in temperature, salinity and other conditions that challenge native protein folds. Therefore, these marine organisms should be ideal for the discovery of molecules that prevent the formation of toxic misfolding. The findings in this study show that *A. esculenta* sampled from the Bay Fundy have compounds capable of altering αS protein fold stability and preventing its amyloid formation. This study also demonstrates the feasibility and practicality of a suite of assays that allow efficient evaluation of extracts from species in these environments for protein folding. This suite of assays can be applied to any potential source of protein folding modulation.

References

National Taiwan Museum: Morphology and Taxonomy of Algae [Internet] [cited 2014 March/25]. Available from: http://formosa.ntm.gov.tw/seaweeds/english/b/b1_01.asp .

Abeliovich A, Schmitz Y, Farinas I, Choi-Lundberg D, Ho W, Castillo P, Shinsky N, Verdugo J, Armanini M, Ryan A, et al. 2000. Mice lacking alpha-synuclein display functional deficits in the nigrostriatal dopamine system. Neuron 25(1):239-52.

Alper T, Cramp WA, Haig DA, Clarke MC. 1967. Does agent of scrapie replicate without nucleic acid. Nature 214(5090):764.

Andrew S, Goldberg Y, Kremer B, Telenius H, Theilmann J, Adam S, Starr E, Squitieri F, Lin B, Kalchman M, et al. 1993. The relationship between trinucleotide (cag) repeat length and clinical-features of huntingtons-disease. Nat Genet 4(4):398-403.

Barbour R, Kling K, Anderson JP, Banducci K, Cole T, Diep L, Fox M, Goldstein JM, Soriano F, Seubert P, et al. 2008. Red blood cells are the major source of alpha-synuclein in blood. Neurodegener Dis 5(2):55-9.

Bartels T, Choi JG, Selkoe DJ. 2011. Alpha-synuclein occurs physiologically as a helically folded tetramer that resists aggregation. Nature 477(7362):107-U123.

Bence NF, Sampat RM, Kopito RR. 2001. Impairment of the ubiquitin-proteasome system by protein aggregation. Science 292(5521):1552-5.

Berson J, Theos A, Harper D, Tenza D, Raposo G, Marks M. 2003. Proprotein convertase cleavage liberates a fibrillogenic fragment of a resident glycoprotein to initiate melanosome biogenesis. J Cell Biol 161(3):521-33.

Bischof K, Hanelt D, Wiencke C. 1999. Acclimation of maximal quantum yield of photosynthesis in the brown alga alaria esculenta under high light and UV radiation. Plant Biology 1(4):435-44.

Bronstein JM, Tagliati M, Alterman RL, Lozano AM, Volkmann J, Stefani A, Horak FB, Okun MS, Foote KD, Krack P, et al. 2011. Deep brain stimulation for parkinson disease an expert consensus and review of key issues. Arch Neurol 68(2):165-71.

Brundin P, Barker RA, Parmar M. 2010. Neural grafting in parkinson's disease problems and possibilities. Prog Brain Res 184:265-94.

Burre J, Sharma M, Tsetsenis T, Buchman V, Etherton MR, Suedhof TC. 2010. Alpha-synuclein promotes SNARE-complex assembly in vivo and in vitro. Science 329(5999):1663-7.

Butterfield DA and Dalle-Donne I. 2012. Redox proteomics. Antioxidants & Redox Signaling 17(11):1487-9.

Cabin D, Shimazu K, Murphy D, Cole N, Gottschalk W, McIlwain K, Orrison B, Chen A, Ellis C, Paylor R, et al. 2002. Synaptic vesicle depletion correlates with attenuated synaptic responses to prolonged repetitive stimulation in mice lacking alpha-synuclein. J Neurosci 22(20):8797-807.

Chen B, Retzlaff M, Roos T, Frydman J. 2011. Cellular strategies of protein quality control. Cold Spring Harbor Perspectives in Biology 3(8):a004374.

Chiti F and Dobson CM. 2006. Protein misfolding, functional amyloid, and human disease. Annu Rev Biochem 75:333-66.

Claessen D, Rink R, de Jong W, Siebring J, de Vreugd P, Boersma F, Dijkhuizen L, Wosten H. 2003. A novel class of secreted hydrophobic proteins is involved in aerial hyphae formation in streptomyces coelicolor by forming amyloid-like fibrils. Genes Dev 17(14):1714-26.

Conway K, Harper J, Lansbury P. 1998. Accelerated in vitro fibril formation by a mutant alpha-synuclein linked to early-onset parkinson disease. Nat Med 4(11):1318-20.

Costanzo M and Zurzolo C. 2013. The cell biology of prion-like spread of protein aggregates: Mechanisms and implication in neurodegeneration. Biochem J 452:1-17.

De Strooper B. 2010. Proteases and proteolysis in alzheimer disease: A multifactorial view on the disease process. Physiol Rev 90(2):465-94.

Deng H, Chen W, Hong S, Boycott KM, Gorrie GH, Siddique N, Yang Y, Fecto F, Shi Y, Zhai H, et al. 2011. Mutations in UBQLN2 cause dominant X-linked juvenile and adult-onset ALS and ALS/dementia. Nature 477(7363):211-U113.

Di Domenico F, Coccia R, Cocciolo A, Murphy MP, Cenini G, Head E, Butterfield DA, Giorgi A, Schinina ME, Mancuso C, et al. 2013. Impairment of proteostasis network in down syndrome prior to the development of alzheimer's disease neuropathology: Redox

proteomics analysis of human brain. Biochim Biophys Acta-Mol Basis Dis 1832(8):1249-59.

Diener T, McKinley M, Prusiner S. 1982. Viroids and prions. Proceedings of the National Academy of Sciences of the United States of America-Biological Sciences 79(17):5220-4.

Douglas PM and Dillin A. 2010. Protein homeostasis and aging in neurodegeneration. J Cell Biol 190(5):719-29.

Drescher M, Huber M, Subramaniam V. 2012. Hunting the chameleon: Structural conformations of the intrinsically disordered protein alpha-synuclein. Chembiochem 13(6):761-8.

Dube A. 2012. Investigation of antifreeze protein activity in blue mussels and amyloid-like transition in a predominant winter flounder serum antifreeze protein. Dalhousie University.

Eanes E and Glenner G. 1968. X-ray diffraction studies on amyloid filaments. J Histochem Cytochem 16(11):673.

Eliezer D, Kutluay E, Bussell R, Browne G. 2001. Conformational properties of alpha-synuclein in its free and lipid-associated states. J Mol Biol 307(4):1061-73.

Fahn S, Shoulson I, Kieburtz K, Rudolph A, Lang A, Olanow CW, Tanner C, Marek K, Parkinson Study Grp. 2004. Levodopa and the progression of parkinson's disease. N Engl J Med 351(24):2498-508.

Fauvet B, Mbefo MK, Fares M, Desobry C, Michael S, Ardah MT, Tsika E, Coune P, Prudent M, Lion N, et al. 2012. Alpha-synuclein in central nervous system and from erythrocytes,

mammalian cells, and escherichia coli exists predominantly as disordered monomer. J Biol Chem 287(19):15345-64.

Feller G and Gerday C. 2003. Psychrophilic enzymes: Hot topics in cold adaptation. Nature Reviews Microbiology 1(3):200-8.

Freshwater D, Fredericq S, Butler B, Hommersand M, Chase M. 1994. A gene phylogeny of the red algae (rhodophyta) based on plastid rbcl. Proc Natl Acad Sci U S A 91(15):7281-5.

Frost B and Diamond MI. 2010. Prion-like mechanisms in neurodegenerative diseases. Nat Rev Neurosci 11(3):155-9.

Fujiwara H, Tabuchi M, Yamaguchi T, Iwasaki K, Furukawa K, Sekiguchi K, Ikarashi Y, Kudo Y, Higuchi M, Saido TC, et al. 2009. A traditional medicinal herb paeonia suffruticosa and its active constituent 1,2,3,4,6-penta-O-galloyl-beta-d-glucopyranose have potent anti-aggregation effects on alzheimer's amyloid beta proteins in vitro and in vivo. J Neurochem 109(6):1648-57.

Giasson B, Murray I, Trojanowski J, Lee V. 2001. A hydrophobic stretch of 12 amino acid residues in the middle of alpha-synuclein is essential for filament assembly. J Biol Chem 276(4):2380-6.

Giunta B, Hou H, Zhu Y, Salemi J, Ruscin A, Shytle RD, Tan J. 2010. Fish oil enhances anti-amyloidogenic properties of green tea EGCG in Tg2576 mice. Neurosci Lett 471(3):134-8.

Glickman M and Ciechanover A. 2002. The ubiquitin-proteasome proteolytic pathway: Destruction for the sake of construction. Physiol Rev 82(2):373-428.

Goate A, Chartierharlin M, Mullan M, Brown J, Crawford F, Fidani L, Giuffra L, Haynes A, Irving N, James L, et al. 1991. Segregation of a missense mutation in the amyloid precursor protein gene with familial alzheimers-disease. Nature 349(6311):704-6.

Goodman Y, Steiner MR, Steiner SM, Mattson MP. 1994. Nordihydroguaiaretic acid protects hippocampal-neurons against amyloid beta-peptide toxicity, and attenuates free-radical and calcium accumulation. Brain Res 654(1):171-6.

Greenfield N and Fasman G. 1969. Computed circular dichroism spectra for evaluation of protein conformation. Biochemistry (N Y) 8(10):4108.

Greenfield NJ. 2006. Using circular dichroism spectra to estimate protein secondary structure. Nature Protocols 1(6):2876-90.

Greville R. 1830. Algae brittannic; or descriptions of the marine and other inarticulated plants of the briish islands belonging to the order algae. 1st ed. Edinburgh: Maclauchlan and Stewart.

AlgalBase - Online Algal Database [Internet]; c2014a [cited 2014 March.25]. Available from: http://www.algaebase.org/ .

The Seaweed Site; Information on marine algae [Internet]; c2014b [cited 2014 March/25]. Available from: http://www.seaweed.ie/descriptions/saccharina_latissima.php .

Guo W, Chen Y, Zhou X, Kar A, Ray P, Chen X, Rao EJ, Yang M, Ye H, Zhu L, et al. 2011. An ALS-associated mutation affecting TDP-43 enhances protein aggregation, fibril formation and neurotoxicity. Nat Struct Mol Biol 18(7):822-U102.

Gupta VB, Indi SS, Rao KSJ. 2009. Garlic extract exhibits antiamyloidogenic activity on amyloid-beta fibrillogenesis: Relevance to alzheimer's disease. Phytotherapy Research 23(1):111-5.

Hochachka P and Somero G. 2002. Temperature. In: Biochemical adaptation: Mechanism and process in physiological evolution. Hochachka P and Somero G, editors. Oxford: Oxford University Press. 290 p.

Hoehn MM and Yahr MD. 1967. Parkinsonism: Onset, progression and mortality. Neurology 17(5):427-42.

Hoffman-Zacharska D, Koziorowski D, Ross OA, Milewski M, Poznanski J, Jurek M, Wszolek ZK, Soto-Ortolaza A, Slawek J, Janik P, et al. 2013. Novel A18T and pA29S substitutions in alpha-synuclein may be associated with sporadic parkinson's disease. Parkinsonism Relat Disord 19(11):1057-60.

Jakes R, Spillantini M, Goedert M. 1994. Identification of 2 distinct synucleins from human brain. FEBS Lett 345(1):27-32.

Jayaraman M, Mishra R, Kodali R, Thakur AK, Koharudin LMI, Gronenborn AM, Wetzel R. 2012. Kinetically competing huntingtin aggregation pathways control amyloid polymorphism and properties. Biochemistry (N Y) 51(13):2706-16.

Kahle P, Neumann M, Ozmen L, Muller V, Jacobsen H, Schindzielorz A, Okochi M, Leimer U, van der Putten H, Probst A, et al. 2000. Subcellular localization of wild-type and parkinson's disease-associated mutant alpha-synuclein in human and transgenic mouse brain. Journal of Neuroscience 20(17):6365-73.

Kang I, Jeon YE, Yin XF, Nam J, You SG, Hong MS, Jang BG, Kim M. 2011. Butanol extract of ecklonia cava prevents production and aggregation of beta-amyloid, and reduces beta-amyloid mediated neuronal death. Food and Chemical Toxicology 49(9):2252-9.

Kang L, Moriarty GM, Woods LA, Ashcroft AE, Radford SE, Baum J. 2012. N-terminal acetylation of alpha-synuclein induces increased transient helical propensity and decreased aggregation rates in the intrinsically disordered monomer. Protein Sci 21(7):911-7.

Kartha G, Bello J, Harker D. 1967. Tertiary structure of ribonuclease. Nature 213(5079):862.

Kelienyi G. 1967. On histochemistry of azo group-free thiazole dyes. J Histochem Cytochem 15(3):172.

Kerman A, Liu H, Croul S, Bilbao J, Rogaeva E, Zinman L, Robertson J, Chakrabartty A. 2010. Amyotrophic lateral sclerosis is a non-amyloid disease in which extensive misfolding of SOD1 is unique to the familial form. Acta Neuropathol 119(3):335-44.

Kirkeby A, Grealish S, Wolf DA, Nelander J, Wood J, Lundblad M, Lindvall O, Parmar M. 2012. Generation of regionally specified neural progenitors and functional neurons from human embryonic stem cells under defined conditions. Cell Reports 1(6):703-14.

PDB Summary: Solution structure of human pancreatic ribonuclease [Internet]; c2011 [cited 2014 02/22]. Available from: http://www.rcsb.org/pdb/explore/explore.do?structureId=2K11 .

Kover KE, Bruix M, Santoro J, Batta G, Laurents DV, Rico M. 2008. The solution structure and dynamics of human pancreatic ribonuclease determined by NMR spectroscopy provide insight into its remarkable biological activities and inhibition. J Mol Biol 379(5):953-65.

Kruger R, Kuhn W, Muller T, Woitalla D, Graeber M, Kosel S, Przuntek H, Epplen J, Schols L, Riess O. 1998. Ala30Pro mutation in the gene encoding alpha-synuclein in parkinson's disease. Nat Genet 18(2):106-8.

Kyle R. 2001. Amyloidosis: A convoluted story. Br J Haematol 114(3):529-38.

Laemmli UK. 1970. Cleavage of structural proteins during assembly of head of bacteriophage-T4. Nature 227(5259):680.

Lashuel HA, Overk CR, Oueslati A, Masliah E. 2013. The many faces of alpha-synuclein: From structure and toxicity to therapeutic target. Nat Rev Neurosci 14(1):38-48.

Lee J, Lee I, Choe Y, Kang S, Kim HY, Gai W, Hahn J, Paik SR. 2009. Real-time analysis of amyloid fibril formation of alpha-synuclein using a fibrillation-state-specific fluorescent probe of JC-1. Biochem J 418:311-23.

Lee J, Hong C, Lee S, Yang J, Park YI, Lee D, Hyeon T, Jung S, Paik SR. 2012. Radiating amyloid fibril formation on the surface of lipid membranes through unit-assembly of oligomeric species of alpha-synuclein. PLoS One 7(10):e47580.

Levine B and Klionsky D. 2004. Development by self-digestion: Molecular mechanisms and biological functions of autophagy. Developmental Cell 6(4):463-77.

LeVine H. 1999. Quantification of beta-sheet amyloid fibril structures with thioflavin T. Amyloid, Prions, and Other Protein Aggregates 309:274-84.

LeVine H. 1993. Thioflavine-T interaction with synthetic alzheimers-disease beta-amyloid peptides - detection of amyloid aggregation in solution. Protein Science 2(3):404-10.

Liou H, Tsai M, Chen C, Jeng J, Chang Y, Chen S, Chen R. 1997. Environmental risk factors and parkinson's disease: A case-control study in taiwan. Neurology 48(6):1583-8.

Lokappa SB and Ulmer TS. 2011. Alpha-synuclein populates both elongated and broken helix states on small unilamellar vesicles. J Biol Chem 286(24):21450-7.

Lotz GP and Legleiter J. 2013. The role of amyloidogenic protein oligomerization in neurodegenerative disease. J Mol Med 91(6):653-64.

Luk KC, Kehm V, Carroll J, Zhang B, O'Brien P, Trojanowski JQ, Lee VM. 2012. Pathological alpha-synuclein transmission initiates parkinson-like neurodegeneration in nontransgenic mice. Science 338(6109):949-53.

Marambaud P, Zhao HT, Davies P. 2005. Resveratrol promotes clearance of alzheimer's disease amyloid-beta peptides. J Biol Chem 280(45):37377-82.

Marchiani A, Mammi S, Siligardi G, Hussain R, Tessari I, Bubacco L, Delogu G, Fabbri D, Dettori MA, Sanna D, et al. 2013. Small molecules interacting with alpha-synuclein: Antiaggregating and cytoprotective properties. Amino Acids 45(2):327-38.

Matulis D, Kranz J, Salemme F, Todd M. 2005. Thermodynamic stability of carbonic anhydrase: Measurements of binding affinity and stoichiometry using ThermoFluor. Biochemistry (N Y) 44(13):5258-66.

McLaurin J, Golomb R, Jurewicz A, Antel JP, Fraser PE. 2000. Inositol stereoisomers stabilize an oligomeric aggregate of alzheimer amyloid beta peptide and inhibit A beta-induced toxicity. J Biol Chem 275(24):18495-502.

Morimoto RI. 2008. Proteotoxic stress and inducible chaperone networks in neurodegenerative disease and aging. Genes Dev 22(11):1427-38.

Nussbaum R and Ellis C. 2003. Genomic medicine: Alzheimer's disease and parkinson's disease. N Engl J Med 348(14):1356-64.

Ono K, Hasegawa KU, Yoshiike Y, Takashima A, Yamada M, Naiki H. 2002. Nordihydroguaiaretic acid potently breaks down pre-formed alzheimer's beta-amyloid fibrils in vitro. J Neurochem 81(3):434-40.

Ono K, Hirohata M, Yamada M. 2007. Anti-fibrillogenic and fibril-destabilizing activity of nicotine in vitro: Implications for the prevention and therapeutics of lewy body diseases. Exp Neurol 205(2):414-24.

Palmer J, Soltis D, Chase M. 2004. The plant tree of life: An overview and some points of view. Am J Bot 91(10):1437-45.

Parmar M and Jakobsson J. 2011. Turning skin into dopamine neurons. Cell Res 21(10):1386-7.

Planchard MS, Exley SE, Morgan SE, Rangachari V. 2014. Dopamine-induced alpha-synuclein oligomers show self- and cross-propagation properties. Protein Sci 23(10):1369-79.

Pokrishevsky E, Grad LI, Yousefi M, Wang J, Mackenzie IR, Cashman NR. 2012. Aberrant localization of FUS and TDP43 is associated with misfolding of SOD1 in amyotrophic lateral sclerosis. PLoS One 7(4):e35050.

Polymeropoulos M, Lavedan C, Leroy E, Ide S, Dehejia A, Dutra A, Pike B, Root H, Rubenstein J, Boyer R, et al. 1997. Mutation in the alpha-synuclein gene identified in families with parkinson's disease. Science 276(5321):2045-7.

Pucciarelli S, La Terza A, Ballarini P, Barchetta S, Yu T, Marziale F, Passini V, Methe B, Detrich HW,III, Miceli C. 2009. Molecular cold-adaptation of protein function and gene regulation: The case for comparative genomic analyses in marine ciliated protozoa. Marine Genomics 2(1):57-66.

Puchtler H, Sweat F, LeVine M. 1962. On binding of congo red by amyloid. Journal of Histochemistry & Cytochemistry 10(3):355.

Rasia R, Bertoncini C, Marsh D, Hoyer W, Cherny D, Zweckstetter M, Griesinger C, Jovin T, Fernandez C. 2005. Structural characterization of copper(II) binding to alpha-synuclein: Insights into the bioinorganic chemistry of parkinson's disease. Proc Natl Acad Sci U S A 102(12):4294-9.

Reid GK, Chopin T, Robinson SMC, Azevedo P, Quinton M, Belyea E. 2013. Weight ratios of the kelps, alaria esculenta and saccharina latissima, required to sequester dissolved inorganic nutrients and supply oxygen for atlantic salmon, salmo salar, in integrated multi-trophic aquaculture systems. Aquaculture 408:34-46.

Rosen D, Siddique T, Patterson D, Figlewicz D, Sapp P, Hentati A, Donaldson D, Goto J, Oregan J, Deng H, et al. 1993. Mutations in cu/zn superoxide-dismutase gene are associated with familial amyotrophic-lateral-sclerosis. Nature 362(6415):59-62.

Schulte PM. 2014. What is environmental stress? insights from fish living in a variable environment. J Exp Biol 217(1):23-34.

Seidler A, Hellenbrand W, Robra B, Vieregge P, Nischan P, Joerg J, Oertel W, Ulm G, Schneider E. 1996. Possible environmental, occupational, and other etiologic factors for parkinson's disease: A case-control study in germany. Neurology 46(5):1275-84.

Serpell L, Sunde M, Benson M, Tennent G, Pepys M, Fraser P. 2000. The protofilament substructure of amyloid fibrils. J Mol Biol 300(5):1033-9.

Shaltiel-Karyo R, Frenkel-Pinter M, Rockenstein E, Patrick C, Levy-Sakin M, Schiller A, Egoz-Matia N, Masliah E, Segal D, Gazit E. 2013. A blood-brain barrier (BBB) disrupter is also a potent alpha-synuclein (alpha-syn) aggregation inhibitor A NOVEL DUAL MECHANISM OF MANNITOL FOR THE TREATMENT OF PARKINSON DISEASE (PD). J Biol Chem 288(24):17579-88.

Sherrington R, Rogaev E, Liang Y, Rogaeva E, Levesque G, Ikeda M, Chi H, Lin C, Li G, Holman K, et al. 1995. Cloning of a gene bearing missense mutations in early-onset familial alzheimers-disease. Nature 375(6534):754-60.

Shvadchak VV, Falomir-Lockhart LJ, Yushchenko DA, Jovin TM. 2011. Specificity and kinetics of alpha-synuclein binding to model membranes determined with fluorescent excited state intramolecular proton transfer (ESIPT) probe. J Biol Chem 286(15):13023-32.

Snell R, Macmillan J, Cheadle J, Fenton I, Lazarou L, Davies P, MacDonald M, Gusella J, Harper P, Shaw D. 1993. Relationship between trinucleotide repeat expansion and phenotypic variation in huntingtons-disease. Nat Genet 4(4):393-7.

Spillantini M, Schmidt M, Lee V, Trojanowski J, Jakes R, Goedert M. 1997. Alpha-synuclein in lewy bodies. Nature 388(6645):839-40.

Storey KB and Storey JM. 2004. Cold hardiness and freeze tolerance. In: Functional metabolism: Regulation and adaptation. Storey KB, editor. John Wiley and Sons, Inc. 473 p.

Sunde M and Blake C. 1997. The structure of amyloid fibrils by electron microscopy and X-ray diffraction. Advances in Protein Chemistry, Vol 50: Protein Misassembly 50:123-59.

Trexler AJ and Rhoades E. 2012. N-terminal acetylation is critical for forming a-helical oligomer of a-synuclein. Protein Sci 21(5):601-5.

Ueda K, Fukushima H, Masliah E, Xia Y, Iwai A, Yoshimoto M, Otero D, Kondo J, Ihara Y, Saitoh T. 1993. Molecular-cloning of cdna-encoding an unrecognized component of amyloid in alzheimer-disease. Proc Natl Acad Sci U S A 90(23):11282-6.

Ulmer T, Bax A, Cole N, Nussbaum R. 2005. Structure and dynamics of micelle-bound human alpha-synuclein. J Biol Chem 280(10):9595-603.

Virchow R. 1854. Ueber eine im gehirn und ruckenmark des menschen aufgefundene substanz mit der chemischen reaction der cellulose. Virchows Arch. Path. Anat. 6:135.

Walters RH and Murphy RM. 2009. Examining polyglutamine peptide length: A connection between collapsed conformations and increased aggregation. J Mol Biol 393(4):978-92.

Webb J, Ravikumar B, Atkins J, Skepper J, Rubinsztein D. 2003. Alpha-synuclein is degraded by both autophagy and the proteasome. J Biol Chem 278(27):25009-13.

Weinreb P, Zhen W, Poon A, Conway K, Lansbury P. 1996. NACP, a protein implicated in alzheimer's disease and learning, is natively unfolded. Biochemistry (N Y) 35(43):13709-15.

Wietek J, Haralampiev I, Amoussouvi A, Herrmann A, Stoeckl M. 2013. Membrane bound alpha-synuclein is fully embedded in the lipid bilayer while segments with higher flexibility remain. FEBS Lett 587(16):2572-7.

Yahr MD, Duvoisin RC, Schear MJ, Barrett RE, Hoehn MM. 1969. Treatment of parkinsonism with levodopa. Arch Neurol 21(4):343.

Yang F, Lim G, Begum A, Ubeda O, Simmons M, Ambegaokar S, Chen P, Kayed R, Glabe C, Frautschy S, et al. 2005. Curcumin inhibits formation of amyloid beta oligomers and fibrils, binds plaques, and reduces amyloid in vivo. J Biol Chem 280(7):5892-901.

Yuan J and Zhao Y. 2013. Evolutionary aspects of the synuclein super-family and sub-families based on large-scale phylogenetic and group-discrimination analysis. Biochem Biophys Res Commun 441(2):308-17.